Neutral 2-phenylbenzimidazole-based iridium(III) complexes with picolinate ancillary ligand: Tuning the emission properties by handling the substituent on the benzimidazole ring

Emiliano Martínez-Vollbert,[a] Christian Philouze[a], Théo Cavignac[b], Camille Latouche[b], Frédérique Loiseau*[a], Pierre-Henri Lanoë*[a]

Experimental details: general consideration

Synthesis

Commercially available reagents were purchased from Sigma-Aldrich, Alfa Aesar, Acros Organics, TCI Chemical, Merck, Strem or Fluorochem and used as received unless otherwise specified. Solvents were obtained from same commercial sources and used without further purification. For moisture sensitive reactions, glassware was oven-dried prior to use. ^{1}H NMR spectra were recorded on a 400 MHz and on a 500 MHz in deuterated solvent ($CDCl_3$, DMSO-d^6 or CD_2Cl_2) and data are reported as follows: chemical shift in ppm from tetramethylsilane with the solvent as an internal indicator ($CDCl_3$ 7.26 ppm, dmso-d^6 2.50 ppm, CD_2Cl_2 5.32 ppm), multiplicity (s = singlet, d = doublet, t = triplet, q = quartet, p = pentet, hept = heptuplet, m = multiplet or overlap of non-equivalent resonances), *J*-coupling constants (Hz), and proton integration. $^{13}C\{^{1}H\}$ NMR spectra were recorded either at 101 MHz or at 126 MHz in suitable deuterated solvent and data are reported as follows: chemical shift in ppm from tetramethylsilane with the solvent as an internal indicator ($CDCl_3$ 77.16 ppm, DMSO-d_6 39.52 ppm, CD_2Cl_2 53.84 ppm). ^{19}F NMR spectra were recorded at 376 MHz and at 470 MHz in the suitable deuterated solvent. ^{31}P NMR spectra were recorded at 202 MHz in the suitable deuterated solvent.

Electrochemistry

Cyclic voltammograms were recorded with a BioLogic SAS potentiostat. All electrochemical measurements were performed in a standard three-compartment electrochemical cell under an argon atmosphere using tetra-*n*-butylammonium hexafluorophosphate ($TBAPF_6$, Aldrich) as supporting electrolyte (0.01 M) in dry CH_3CN. Silver/silver nitrate (ANE2) in CH_3CN ($Ag/AgNO_3$ 10 mM in CH_3CN) and a platinum coil were used as reference and counter electrodes, respectively). 5 mm diameter vitreous carbon electrodes were used as working electrodes.

Absorption and emission spectroscopies

Absorption spectra were recorded on a Cary 300 UV−visible spectrophotometer (Varian) and emission spectra (in solution at room temperature and in rigid matrix at 77 K) were recorded on a Horiba Fluoromax 4. Quartz cuvettes with 1 cm optical path were used. Lifetimes were measured using LP900 spectrometer with a Flashlamp pumped by Q-switched Nd:Yag laser operating at 355 nm and with a photomulitplier (PMT) detector, or with a picosecond laser diode operating at 410 nm and using a time-correlated single photon counting detection (TCSPC, PicoHarp 300).

Emission quantum yields in solution were determined in deaerated CH_2Cl_2 or CH_3CN solutions at room temperature, and calculated with the following equation.

$$QY_s = QY_{ref} X \frac{I_s}{I_{ref}} X \frac{A_{ref}}{A_s} X \left(\frac{\eta_s}{\eta_{ref}}\right)^2$$

QY_s corresponds to the quantum yield of the sample to be analysed, **QY_{ref}** is the quantum yield of the reference compound (in this work is $Ir(ppy)_3$ in deaerated CH_2Cl_2 solution with value of 0.46), **I** corresponds to the intensity of the emission (area of the spectrum), **A** is the absorption at the excitation wavelength, **η** corresponds to the refractive index of the solvents.

Solid-state emission spectra were obtained on a Horiba-Jobin-Yvon Fluorolog-3® spectrofluorimeter, equipped with a three-slit double-grating excitation and emission monochromator with dispersions of 2.1 nm.mm-1 (1200 grooves mm-1 and a R928 photodetector). Samples were introduced into an open capillary quartz tube, which was placed into the cavity of a GMP G8 integration sphere.

The two properties that provide information about the excited state beside the shape of the emission are the **QY** (Φ) and lifetime (τ), represented the following equations.

$$\Phi = \frac{k_r}{k_r + k_{nr}} \quad \tau = \frac{1}{k_r + k_{nr}}$$

The radiative (k_r) and non radiative (k_r) constants can obtained from combination and rearrengment of the **QY** (Φ) and τ equations to give equations:

$$k_r = \frac{\Phi}{\tau} \qquad k_{nr} = \frac{1}{\tau} - k_r$$

Crystal Structures Determinations and Refinements.

Single crystals of compounds **$IrL^6{}_2pic$**, **$IrL^9{}_2pic$** and **$IrL^{10}{}_2pic$**, were picked up from the mother liquor, coated with a parafin mixture, collected with nylon loops and mounted on goniometer heads. Measurements were made at 200 K on a Enraf-Nonius 4 circles kappa goniometer equipped with an Incoatec high brilliance microsource with Montel optics monochromated Mo-

Kα radiation (λ = 0.71073 Å). The detector was a Bruker APEXII and an Oxford Cryosystem cryostream cooler was used. The crystal data and details of the data collections are given in Table S 1. The data were integrated and corrected for Lorentz and polarization effects using Eval14[i], corrected for absorption using SADABS[ii] and finaly merged using Xprep[iii]. Crystallographic structures were solved using direct methods implemented by Superflip.[iv] Refinement was performed using ShelxL-2013[v] run under Olex2[vi]. C, Cl, F, Ir, N, O, and Br atoms were refined anisotropically by the full matrix least-squares method on F^2. H atoms were set geometrically.

Supplementary data is available on request from the CCDC, 12 Union Road, Cambridge CB2 1EZ, UK, quoting the deposition number CCDC-2246643, -2246644 and -2246645 for **IrL$^6_2$pic**, **IrL$^9_2$pic** and **IrL$^{10}_2$pic** respectively. These data can be obtained free of charge at www.ccdc.cam.ac.uk/conts/retrieving.html or fax: +44-1223/336-033; E-mail: deposit@ccdc.cam.ac.uk].

Table S 1 : Crystal data and structure refinement.

Compound	**IrL$^6_2$pic** / CCDC 2246643	**IrL$^9_2$pic** / CCDC 2246644	**IrL$^{10}_2$pic** / CCDC 2246645
Formula	$C_{42}H_{36}F_6IrN_5O_4$	$C_{40}H_{32}F_6IrN_5O_2$. (CH_2Cl_2)	$C_{42}H_{36}F_6IrN_5O_4$. 1.54(CH_2Cl_2)
F_w	980.96	1005.83	1112.05
T [K]	200	200	200
Morphology	needle	block	block
Color	yellow	yellow	orange
Crystal size [mm]	0.10 x 0.17 x 0.40	0.24 x 0.24 x 0.43	0.14 x 0.28 x 0.32
Crystal system	triclinic	monoclinic	monoclinic
Space group	P -1	P 2_1/n	P 2_1/n
a [Å]	11.392(2)	16.113(3)	15.316(3)
b [Å]	11.878(2)	15.027(3)	15.544(3)
c [Å]	14.728(3)	17.152(3)	19.688(4)
α [°]	85.63(3)	90	90
β [°]	88.84(3)	102.83(3)	101.07(3)
γ [°]	78.87(3)	90	90
Unit-cell volume [Å^3]	1949.7(7)	4049.4(15)	4600.0(17)
Z	2	4	4

[i] Duisenberg, A. J. M., Kroon-Batenburg, L. M. J. & Schreurs, A. M. M. (2003). *J. Appl. Cryst*. **36**, 220-229.
[ii] Bruker (2004). *SADABS.* Bruker AXS Inc., Madison, Wisconsin, USA.
[iii] Bruker (2005). *XPREP.* Bruker AXS Inc., Madison, Wisconsin, USA.
[iv] Palatinus, L. & Chapuis, G. (2007). *J. Appl. Cryst.* **40**, 786-790.
[v] Sheldrick, G. M. (2015). *Acta Cryst.* C**71**, 3-8.
[vi] Dolomanov, O.V., Bourhis, L.J., Gildea, R.J, Howard, J.A.K. & Puschmann, H. (2009), J. Appl. Cryst. 42, 339-341

D_x [g·cm^{-3}]	1.671	1.650	1.606
μ [mm^{-1}]	3.502	3.499	3.153
Radiation [Å]	MoKα (λ = 0.71073)	MoKα (λ = 0.71073)	MoKα (λ = 0.71073)
Θ range for data collection/°	2.296 to 30.000	2.388 to 27.500	2.283 to 27.500
Index ranges	-16 ≤ h ≤ 16, -16 ≤ k ≤ 16, -20 ≤ l ≤ 20	-20 ≤ h ≤ 20, -19 ≤ k ≤ 19, -22 ≤ l ≤ 22	-19 ≤ h ≤ 19, -20 ≤ k ≤ 19, -23 ≤ l ≤ 25
Total reflections	45506	50004	62266
Unique reflections	11358	9220	10403
Used reflections (I>2σ(I))	10433	7389	8712
Refined parameters	605	584	650
Rint.	0.0305	0.0338	0.0615
R^a	0.0197	0.0324	0.0366
$R(w)^a$	0.0442	0.0729	0.0899
Goodness of fit *S*	1.167	1.155	1.132
$\Delta\rho_{min}/\Delta\rho_{max}$ (e·Å^{-3})	-0.886/1.247	-2.215/2.185	-1.772/1.950

[a] Refinement based on F^2 where

$w = 1/[\sigma^2(Fo^2)+(0.0157P)^2+1.1400P]$ where $P=(Fo^2+2Fc^2)/3$ for CCDC-2246643

$w = 1/[\sigma^2(Fo^2)+(0.0247P)^2+17.9483P]$ where $P=(Fo^2+2Fc^2)/3$ for CCDC-2246644

$w = 1/[\sigma^2(Fo^2)+(0.0411P)^2+12.1613P]$ where $P=(Fo^2+2Fc^2)/3$ for CCDC-2246645

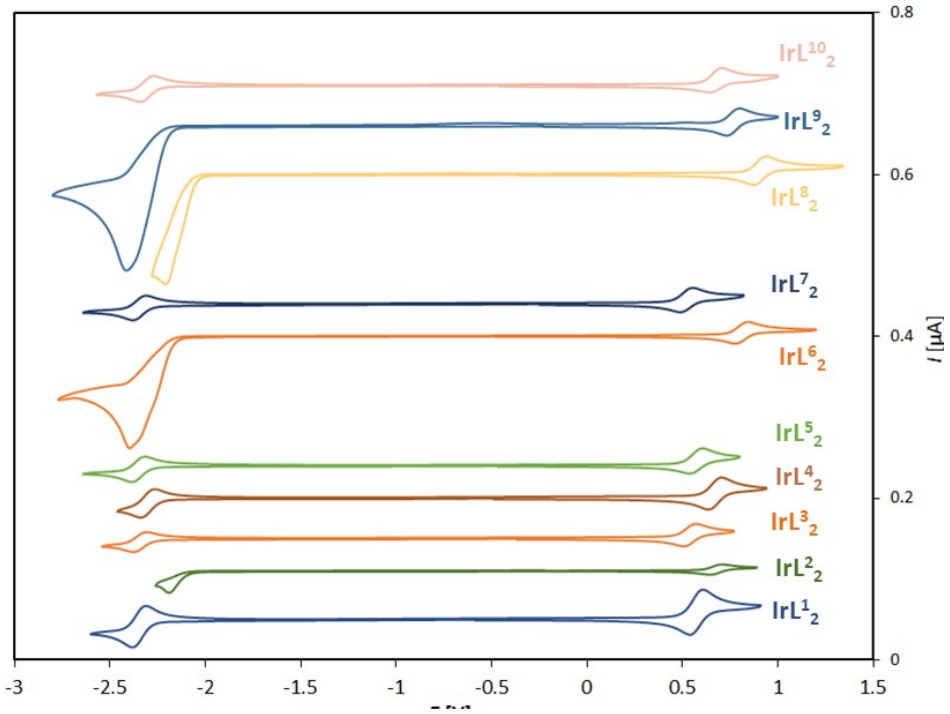

Figure S 1 :*Cyclic voltammograms of the complexes (10^{-3} M to the exception of **IrL^3_2** see below) in deaerated CH_3CN, containing 0.1 M of n-BuN_4PF_6, at a scan rate of 100 mV.s^{-1} using vitreous carbon working electrode (5 mm diameter), E(V) vs Ag/$AgNO_3$ (0.01 M). **IrL^3_2** displays low solubility in the solvent (CH_3CN) that leads to lower current during the experiment and the CV was performed in a saturated solution.*

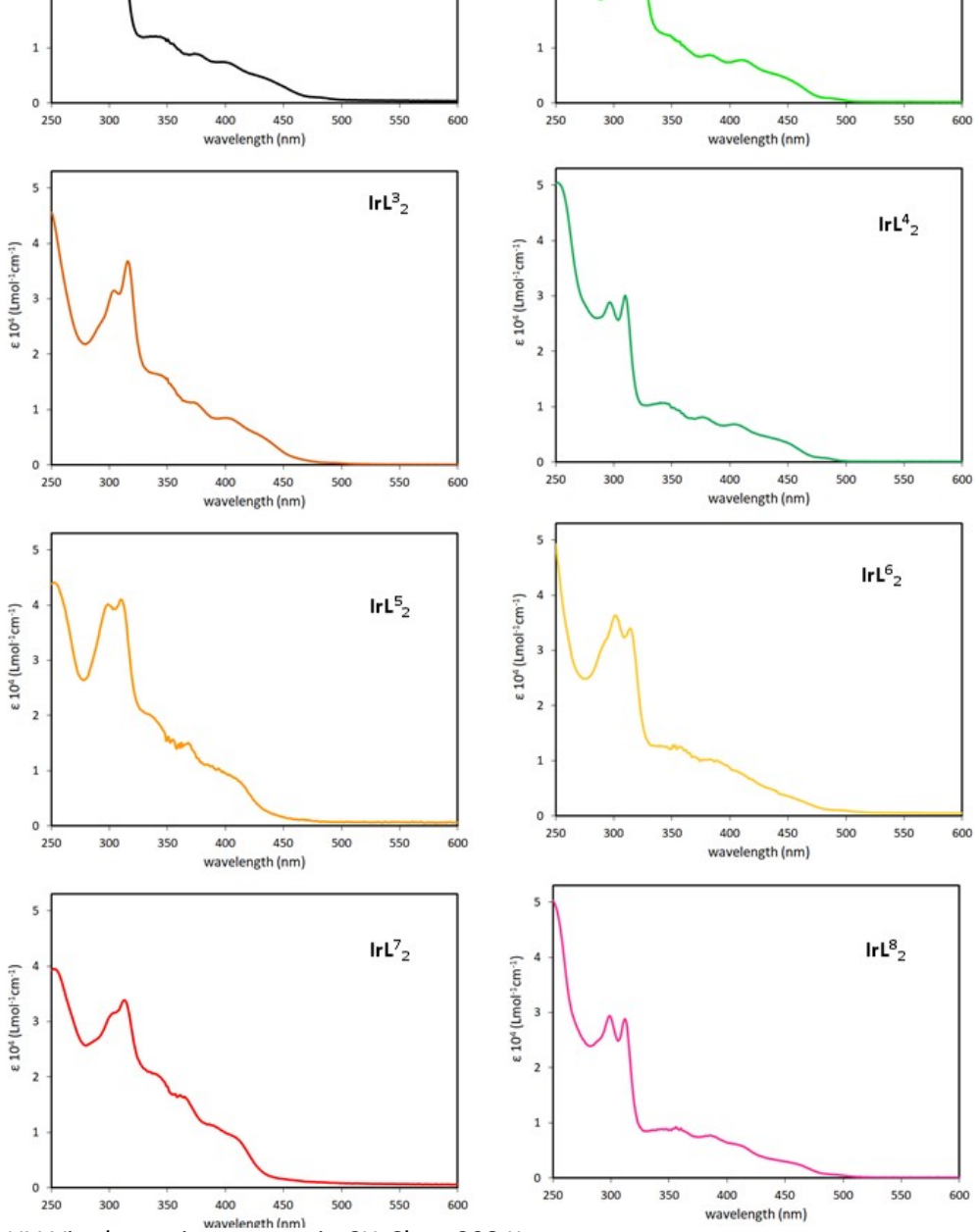

Figure S 2: UV-Vis absorption spectra in CH_2Cl_2 at 298 K

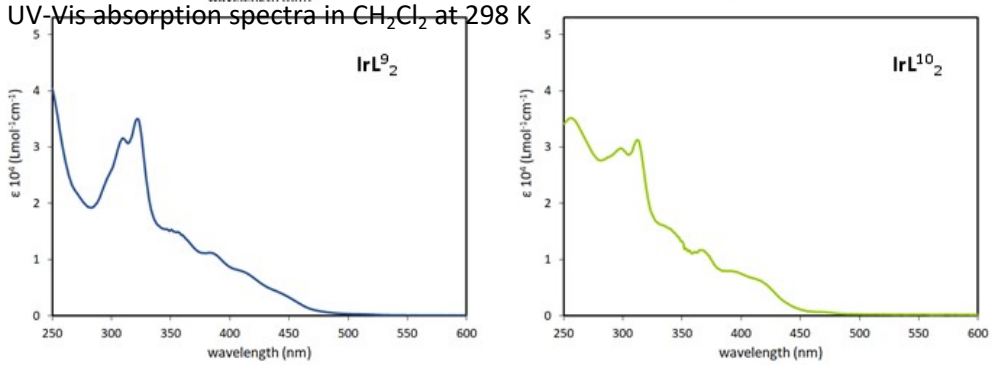

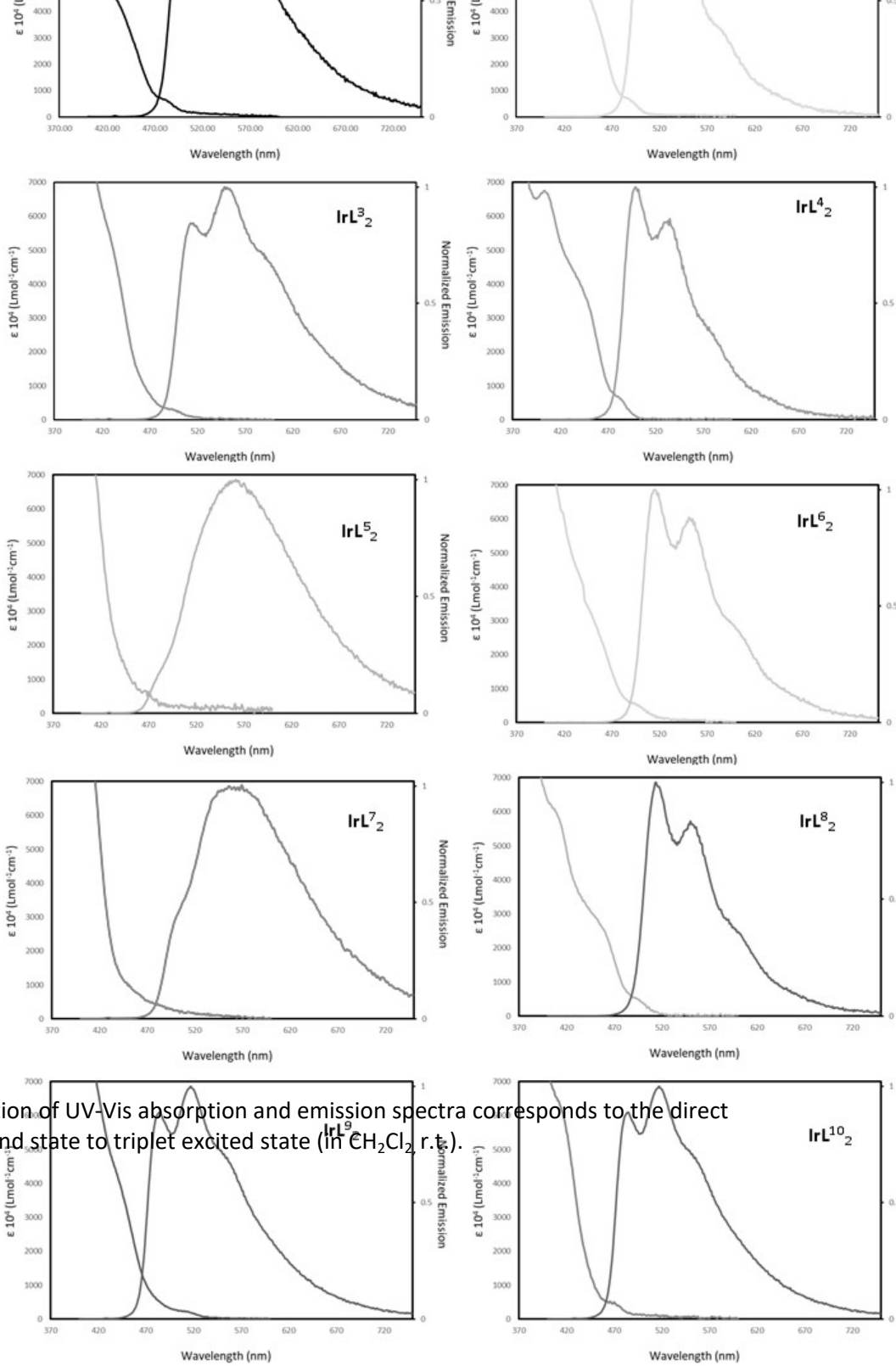

Figure S 3 : The superimposition of UV-Vis absorption and emission spectra corresponds to the direct absorption from singlet ground state to triplet excited state (in CH_2Cl_2 r.t.).

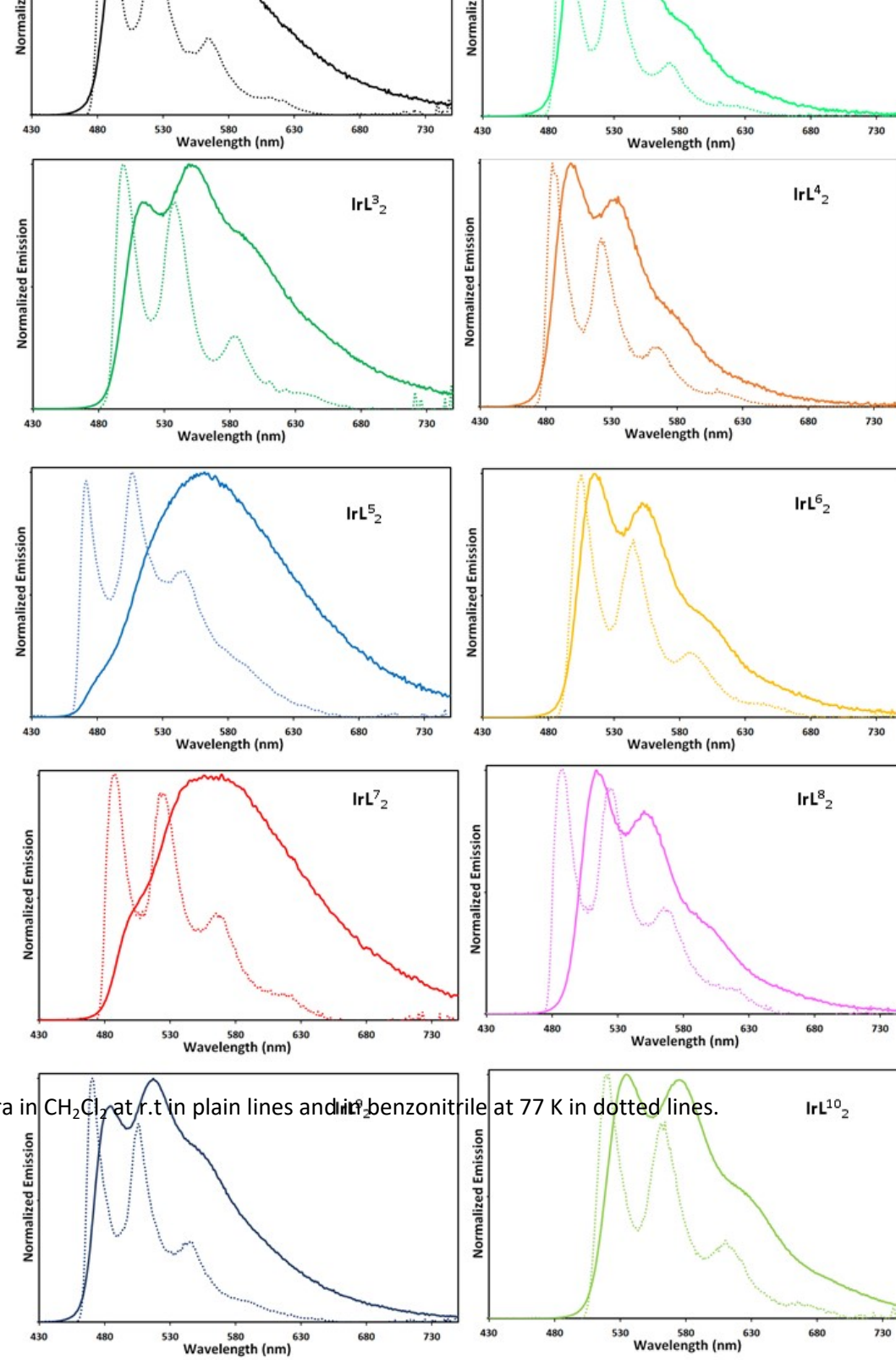

Figure S 4 : Emission spectra in CH_2Cl_2 at r.t in plain lines and in benzonitrile at 77 K in dotted lines.

NMR spectra

IrL^1_2

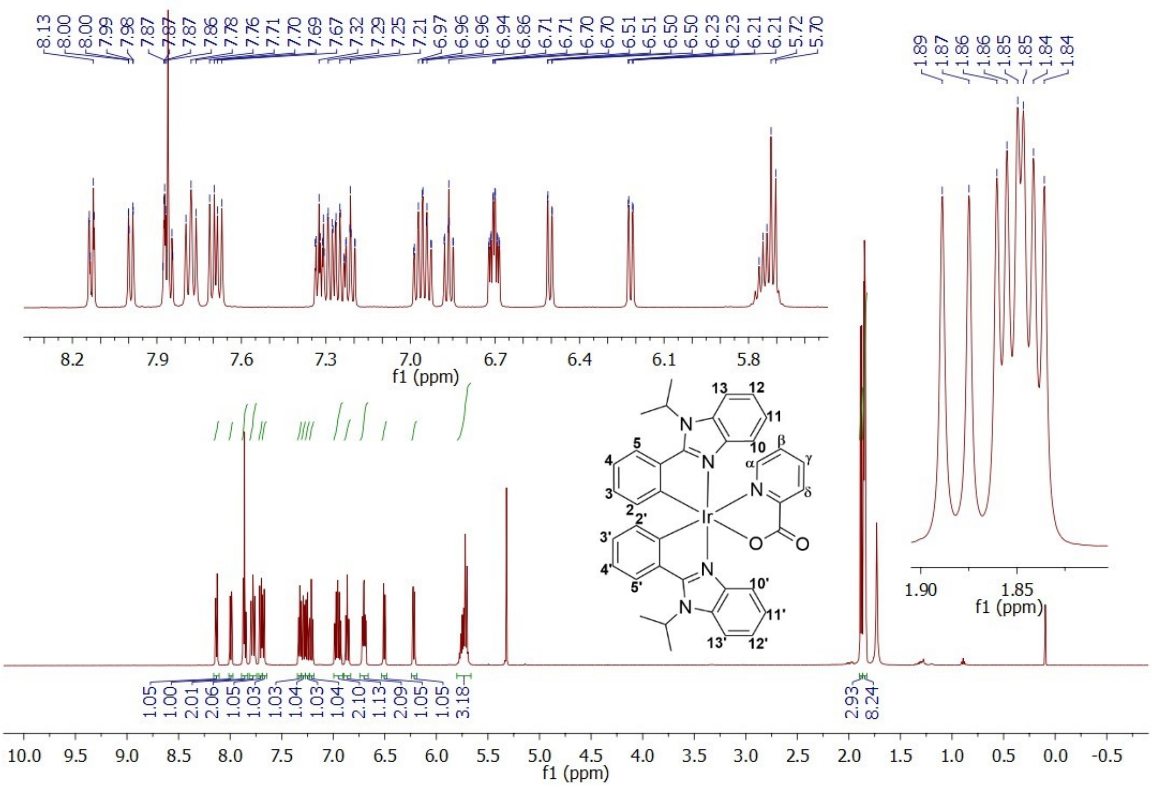

Figure S 5: ^{1}H NMR spectra (500 MHz, CD_2Cl_2)

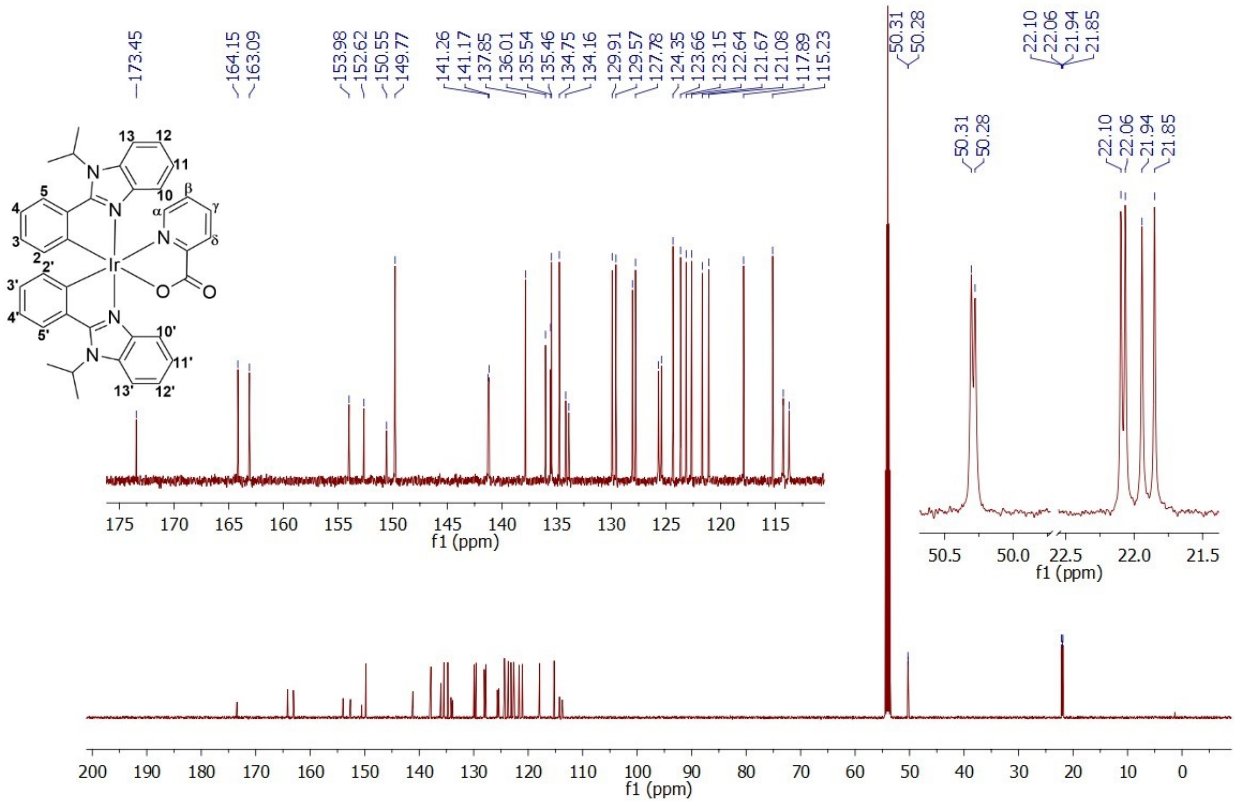

Figure S 6: ^{13}C NMR spectra (500 MHz, CD_2Cl_2)

IrL^2_2

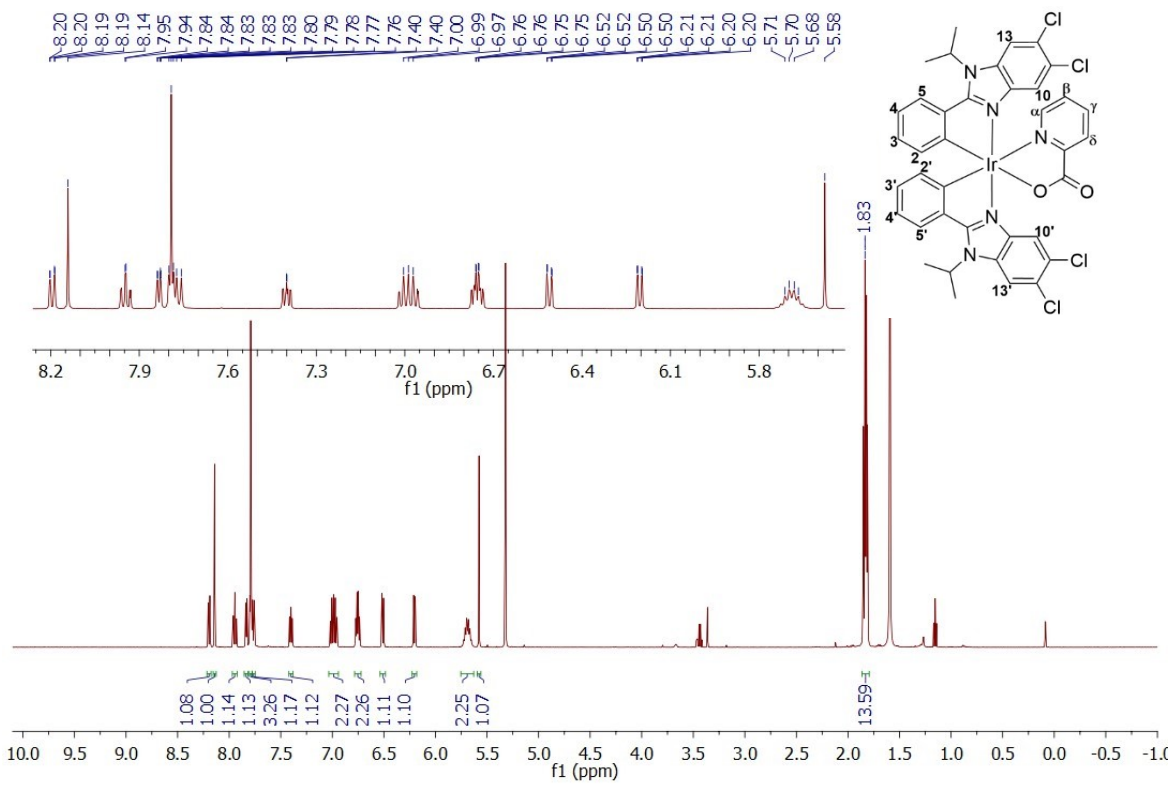

Figure S 7: ^{1}H NMR spectra (500 MHz, CD_2Cl_2)

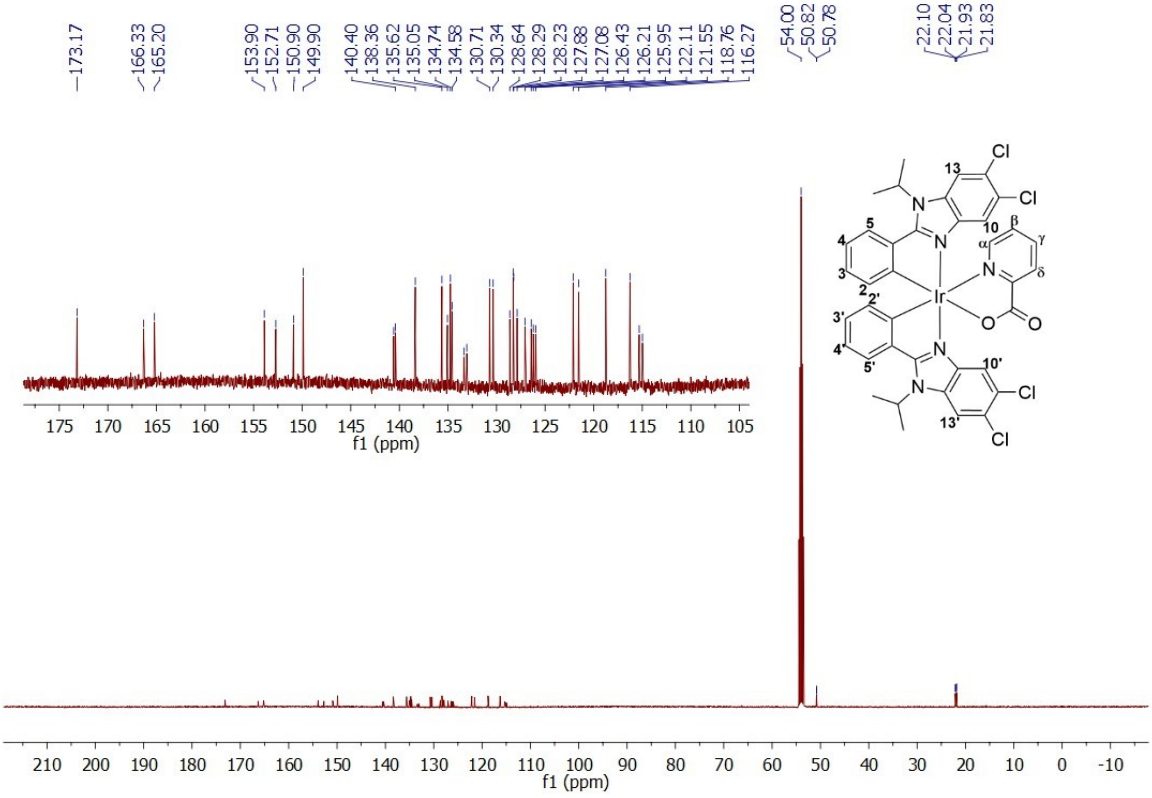

Figure S 8: ^{13}C NMR spectra (500 MHz, CD_2Cl_2)

IrL^3_2

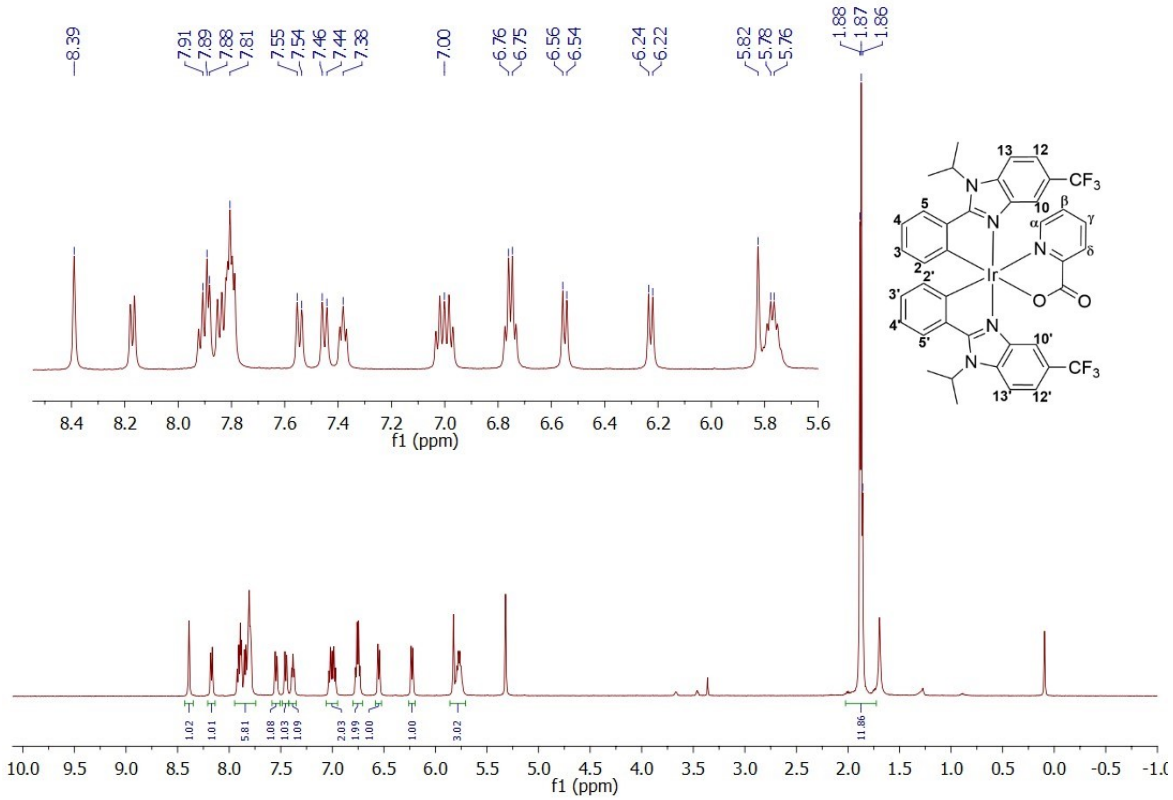

Figure S 9: ^{1}H NMR spectra (500 MHz, CD_2Cl_2)

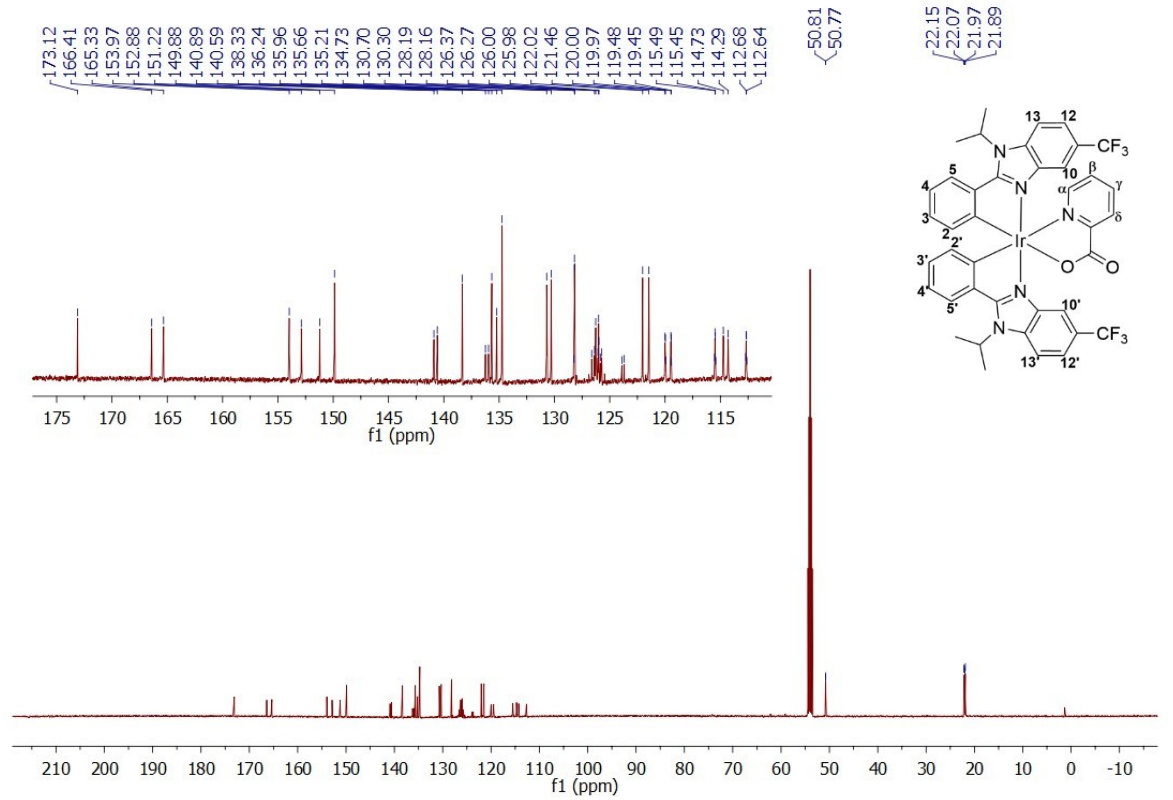

Figure S 10: ^{13}C NMR spectra (500 MHz, CD_2Cl_2)

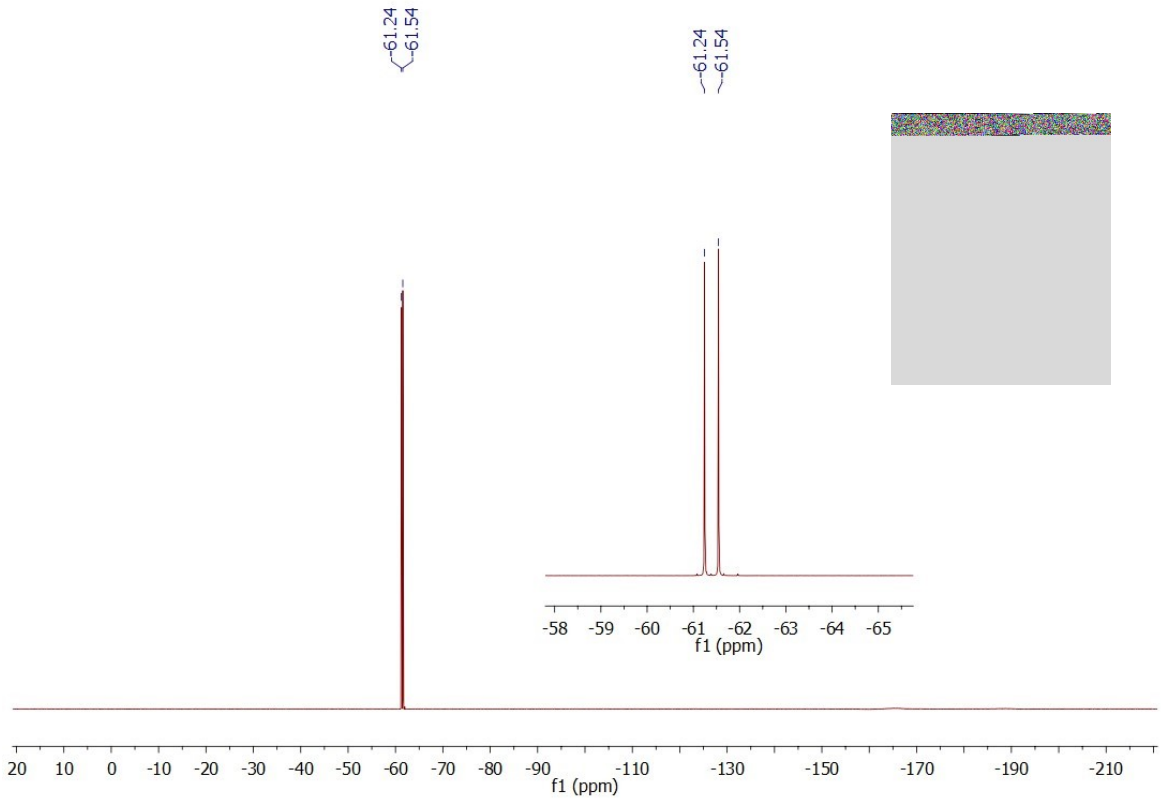

Figure S 11: ^{19}F NMR spectra (500 MHz, CD_2Cl_2)

IrL^4_2

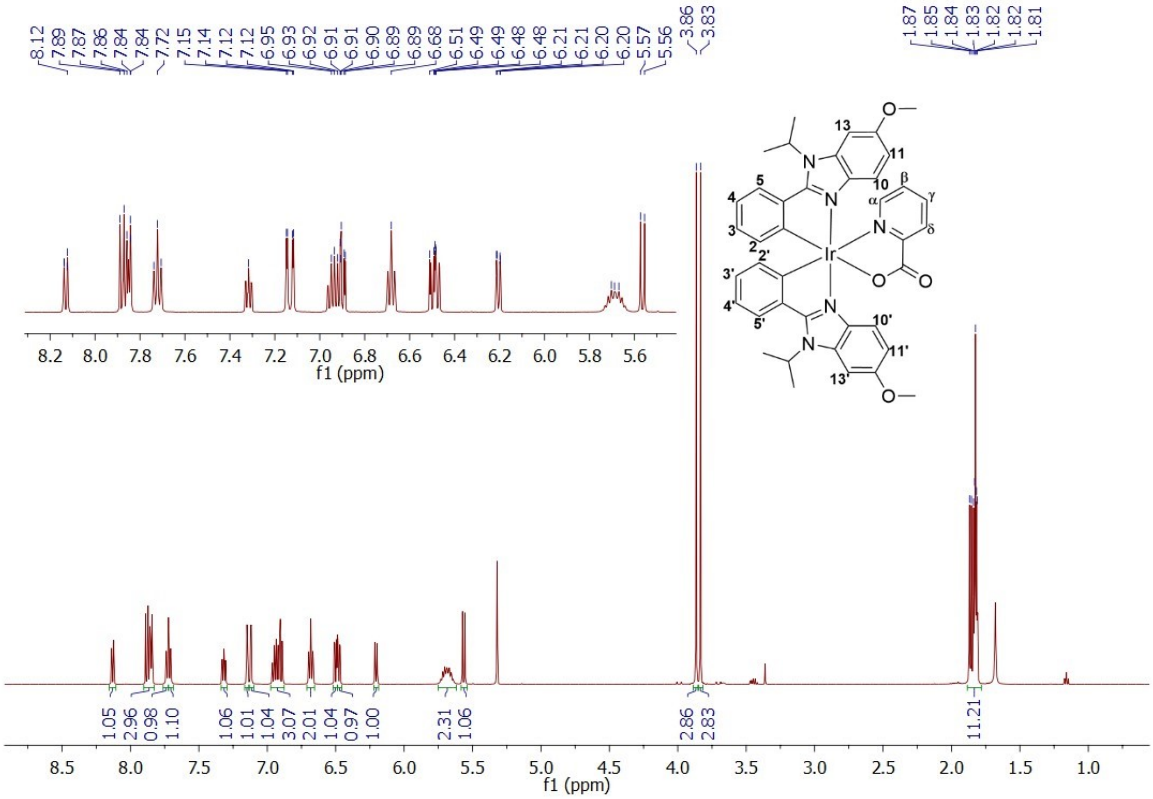

Figure S 12: ^{1}H NMR spectra (500 MHz, CD_2Cl_2)

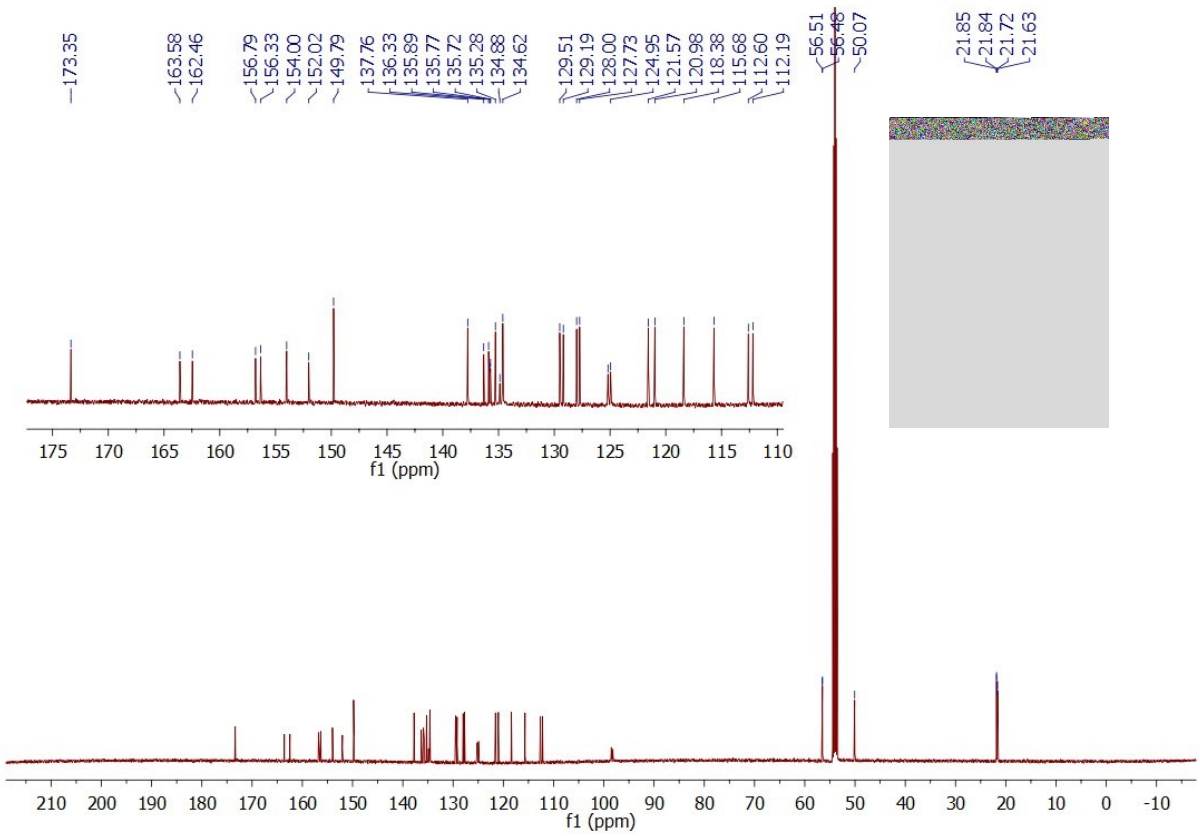

Figure S 13: ^{13}C NMR spectra (500 MHz, CD_2Cl_2)

IrL^5_2

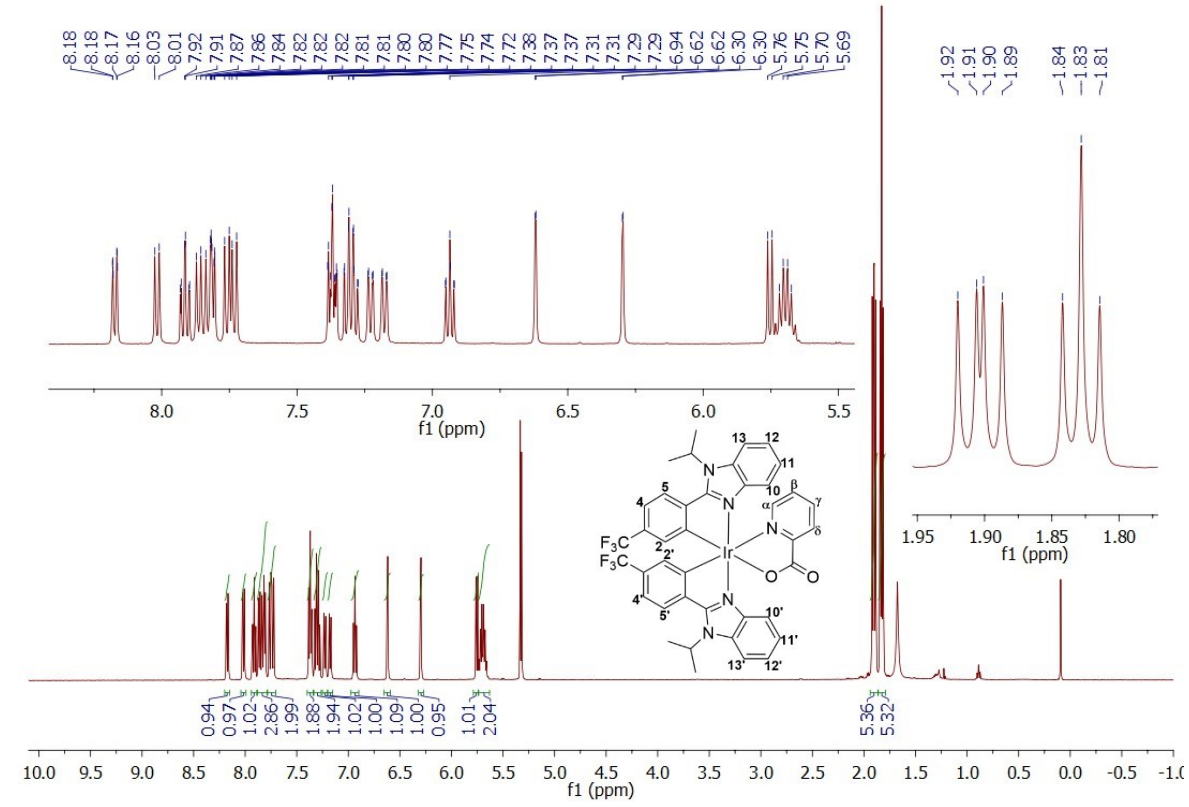

Figure S 14: ^{1}H NMR spectra (500 MHz, CD_2Cl_2)

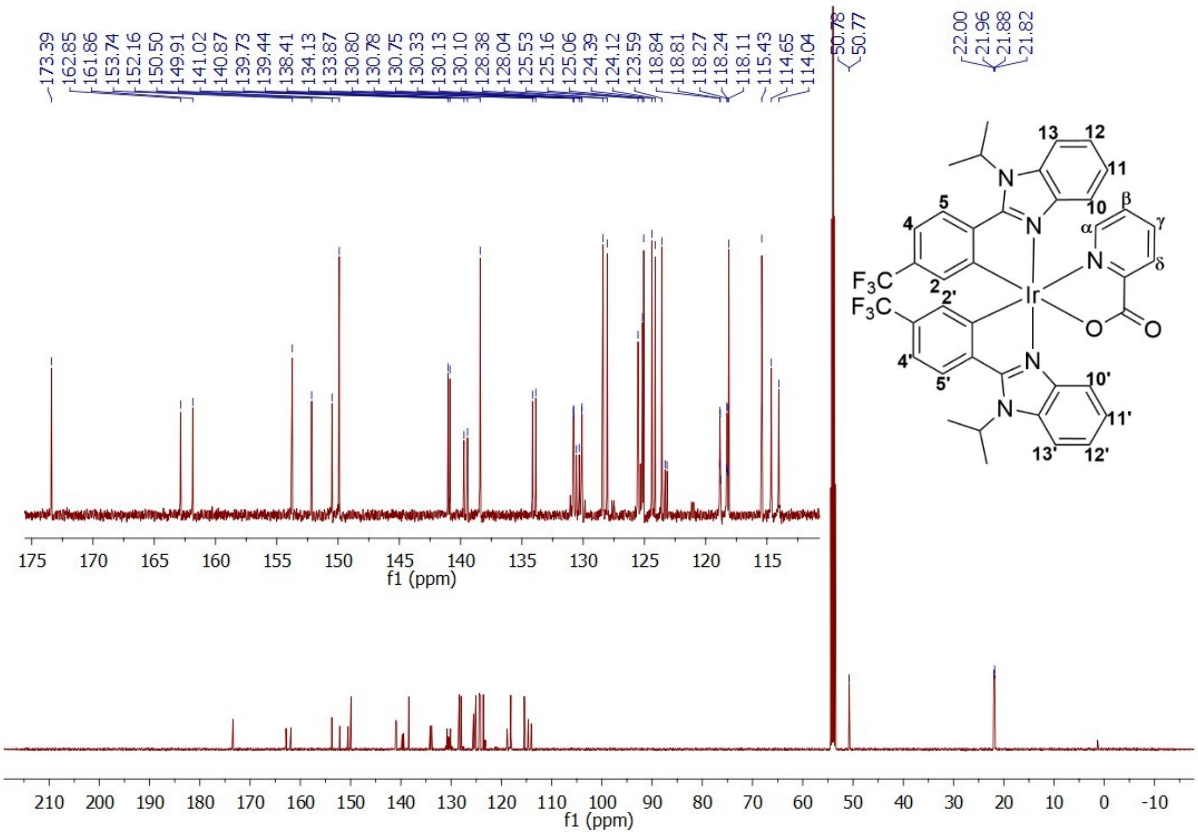

Figure S 15: ^{13}C NMR spectra (500 MHz, CD_2Cl_2)

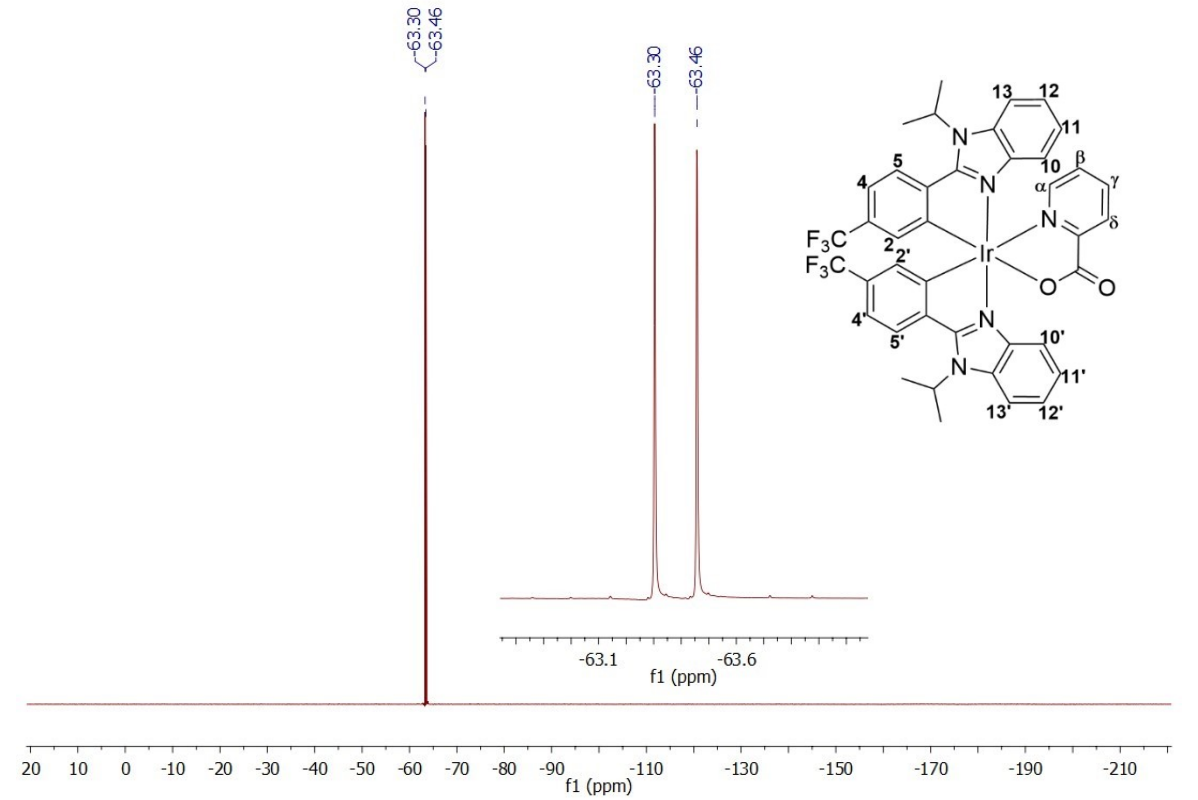

Figure S 16: ^{19}F NMR spectra (500 MHz, CD_2Cl_2)

IrL^6_2

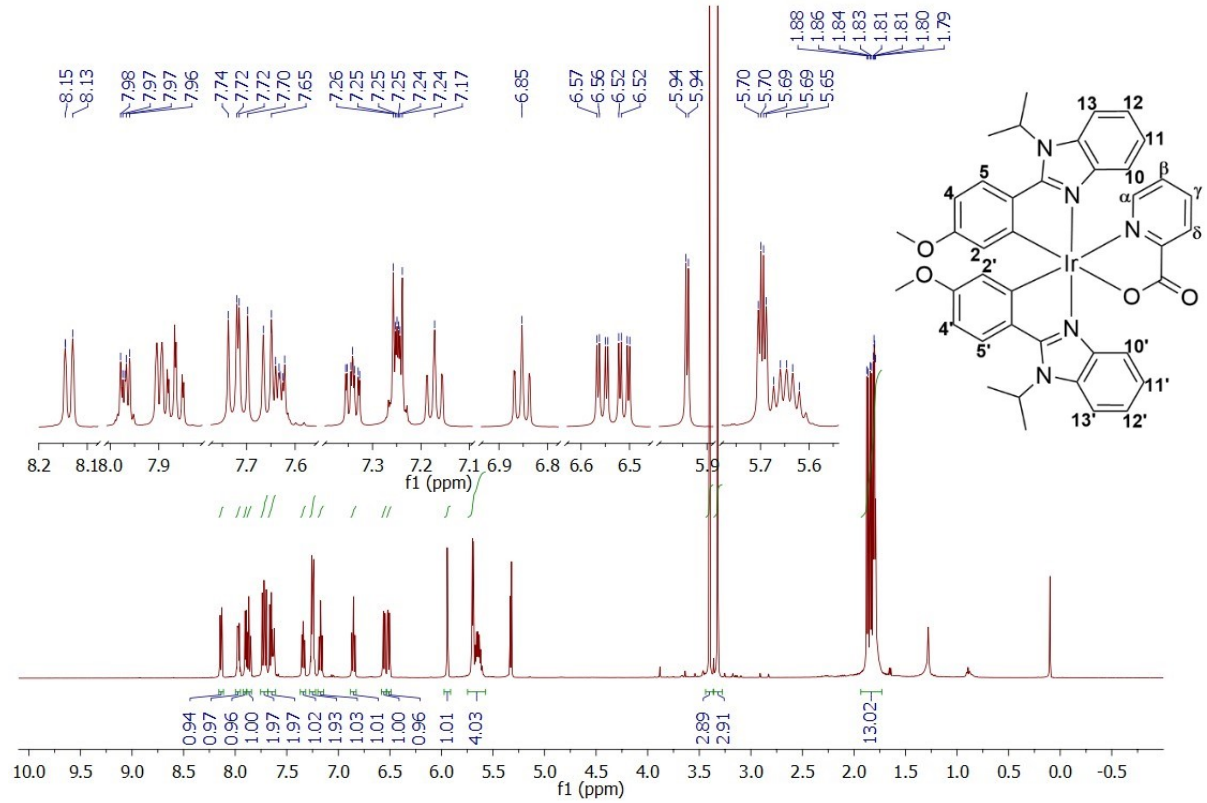

Figure S 17: ^{1}H NMR spectra (500 MHz, CD_2Cl_2)

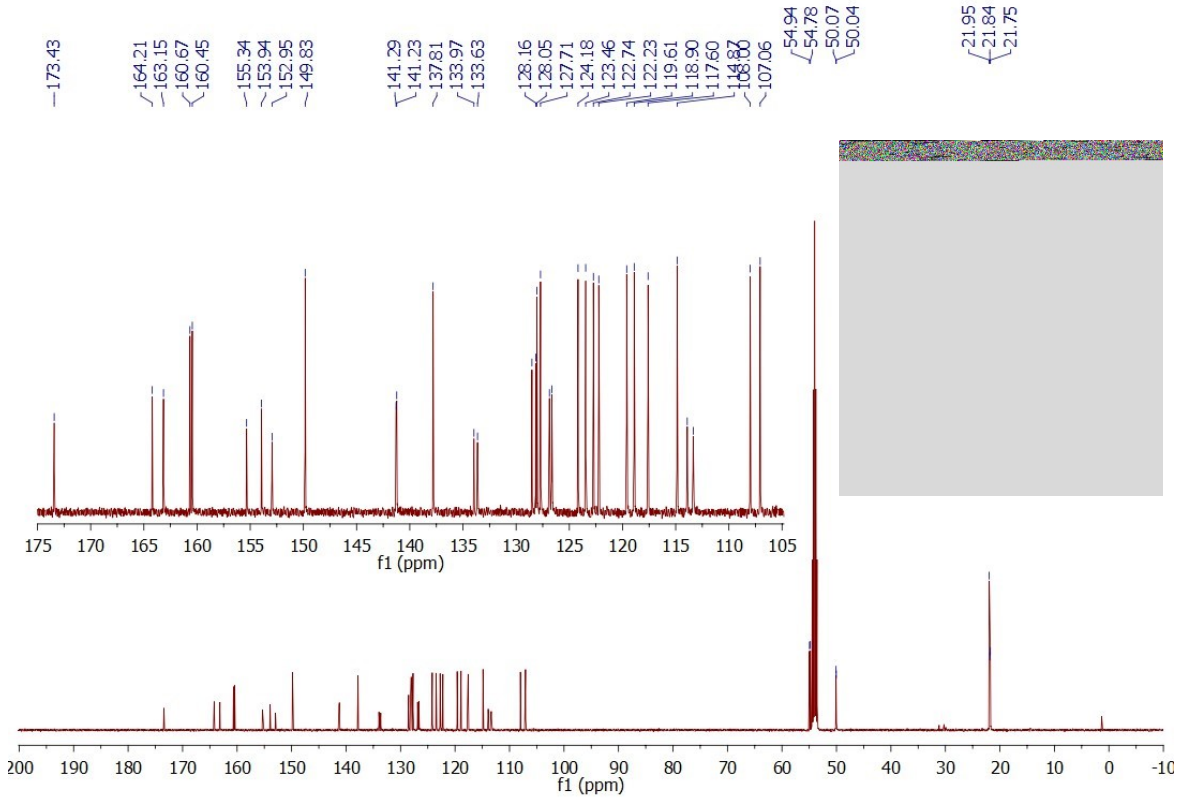

Figure S 18: ^{13}C NMR spectra (500 MHz, CD_2Cl_2)

IrL^7_2

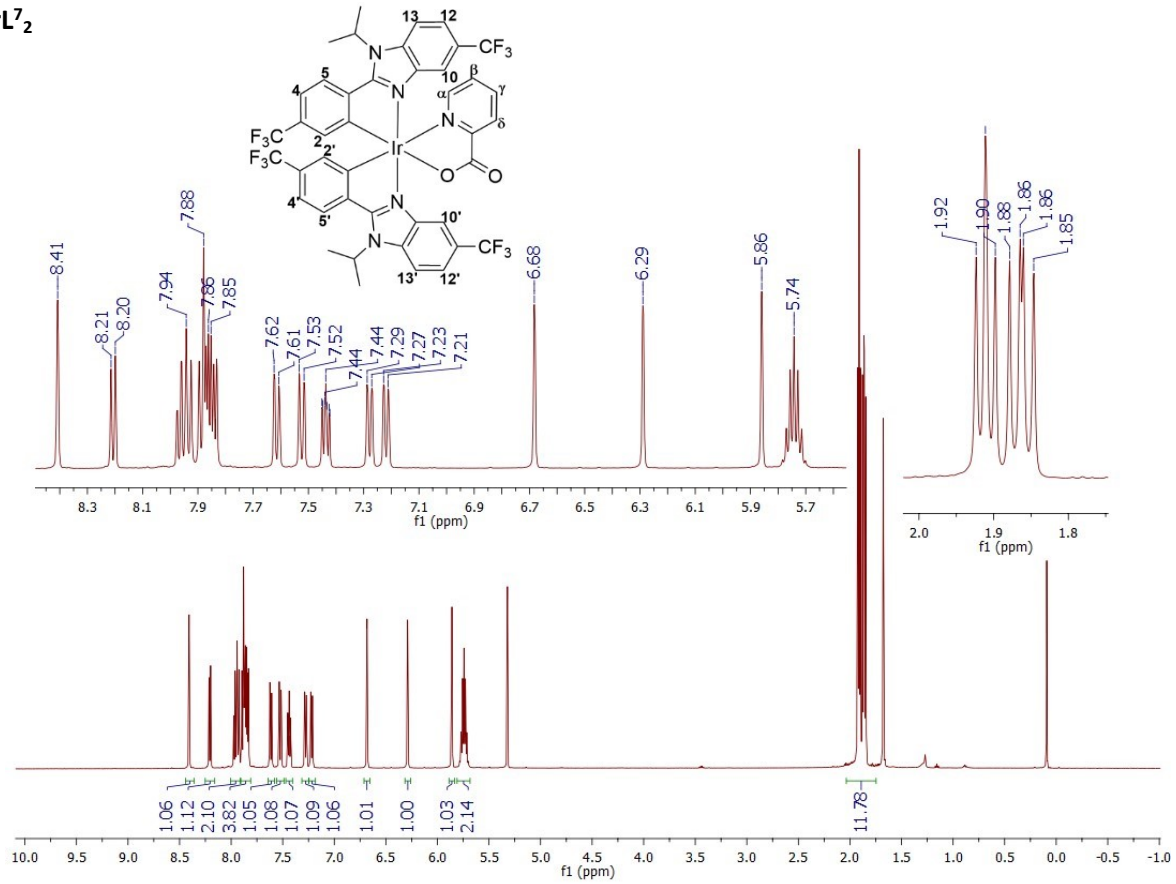

Figure S 19: ^{1}H NMR spectra (500 MHz, CD_2Cl_2)

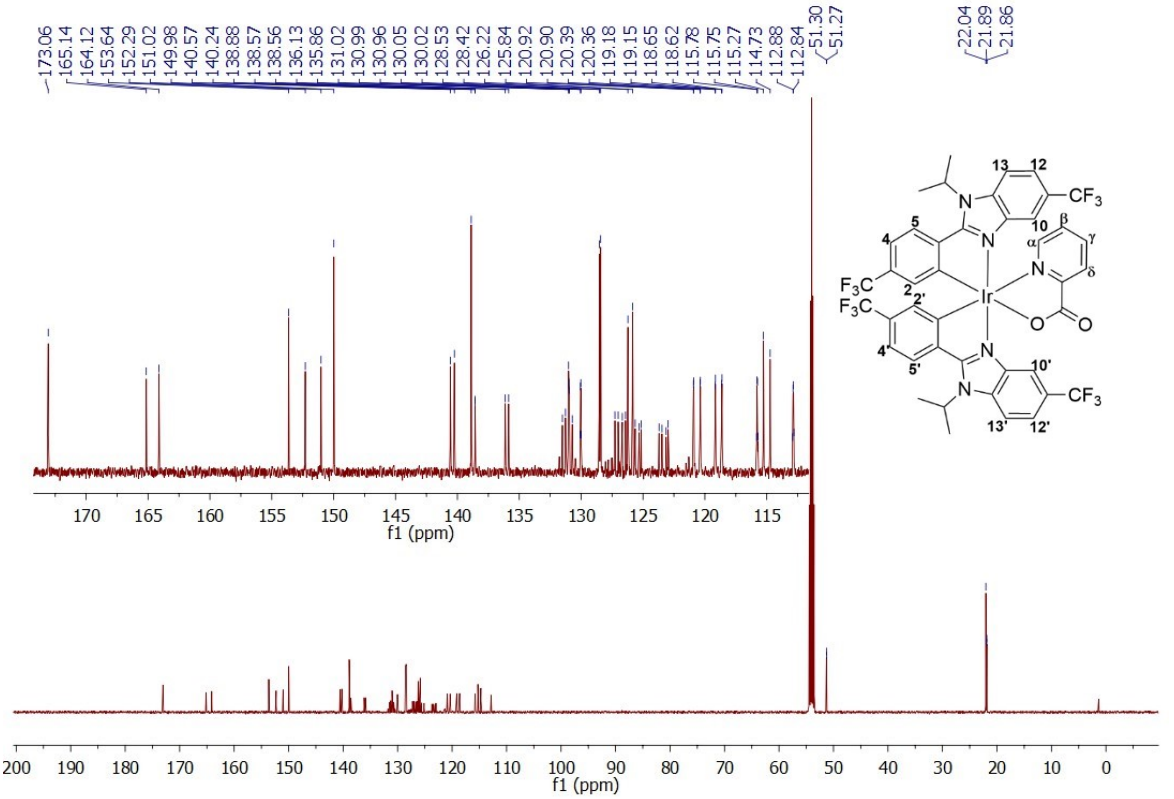

Figure S 20: ^{13}C NMR spectra (500 MHz, CD_2Cl_2)

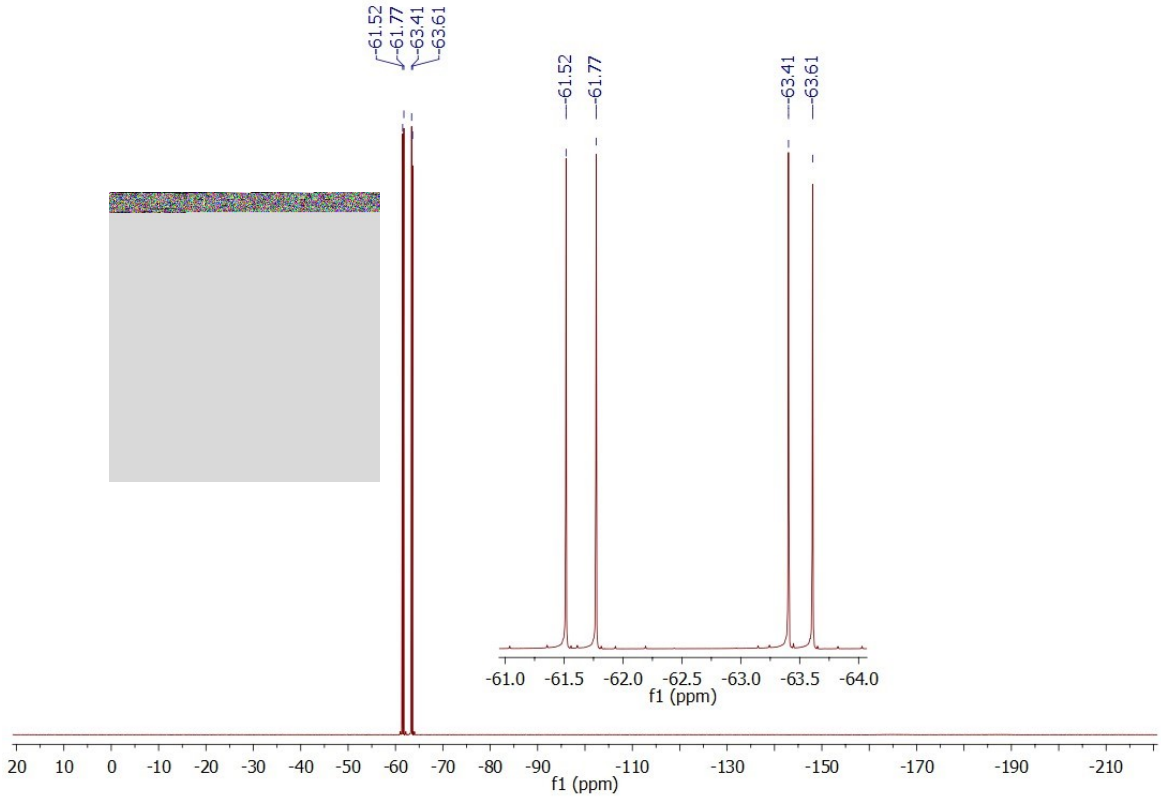

Figure S 21: ^{19}F NMR spectra (500 MHz, CD_2Cl_2)

IrL^8_2

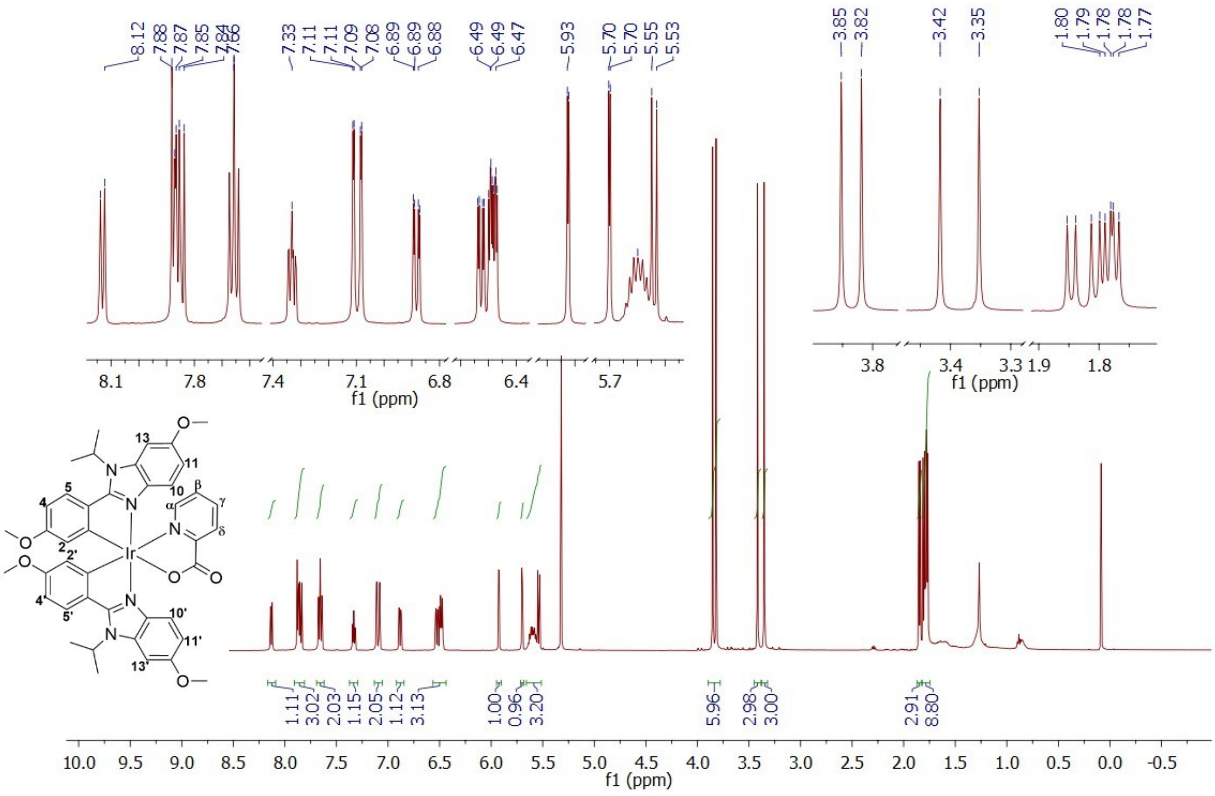

Figure S 22: ^{1}H NMR spectra (500 MHz, CD_2Cl_2)

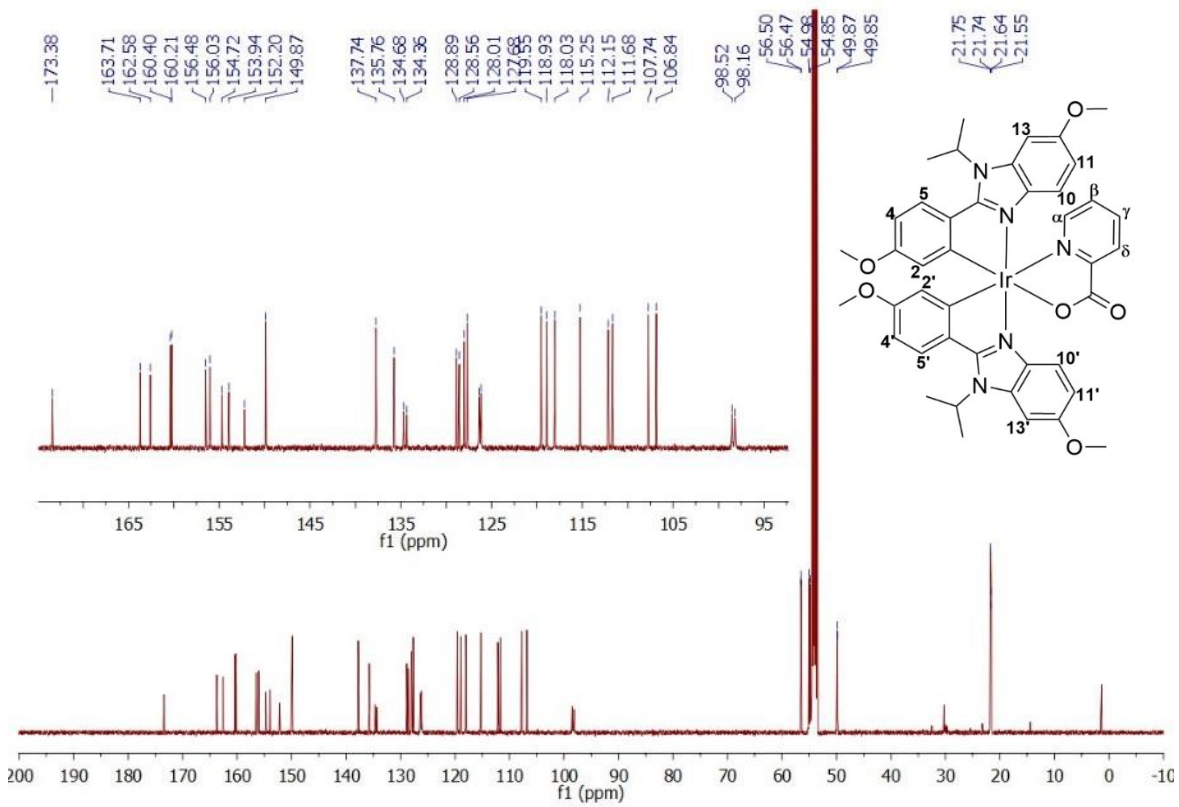

Figure S 23: ^{13}C NMR spectra (500 MHz, CD_2Cl_2)

IrL^9_2

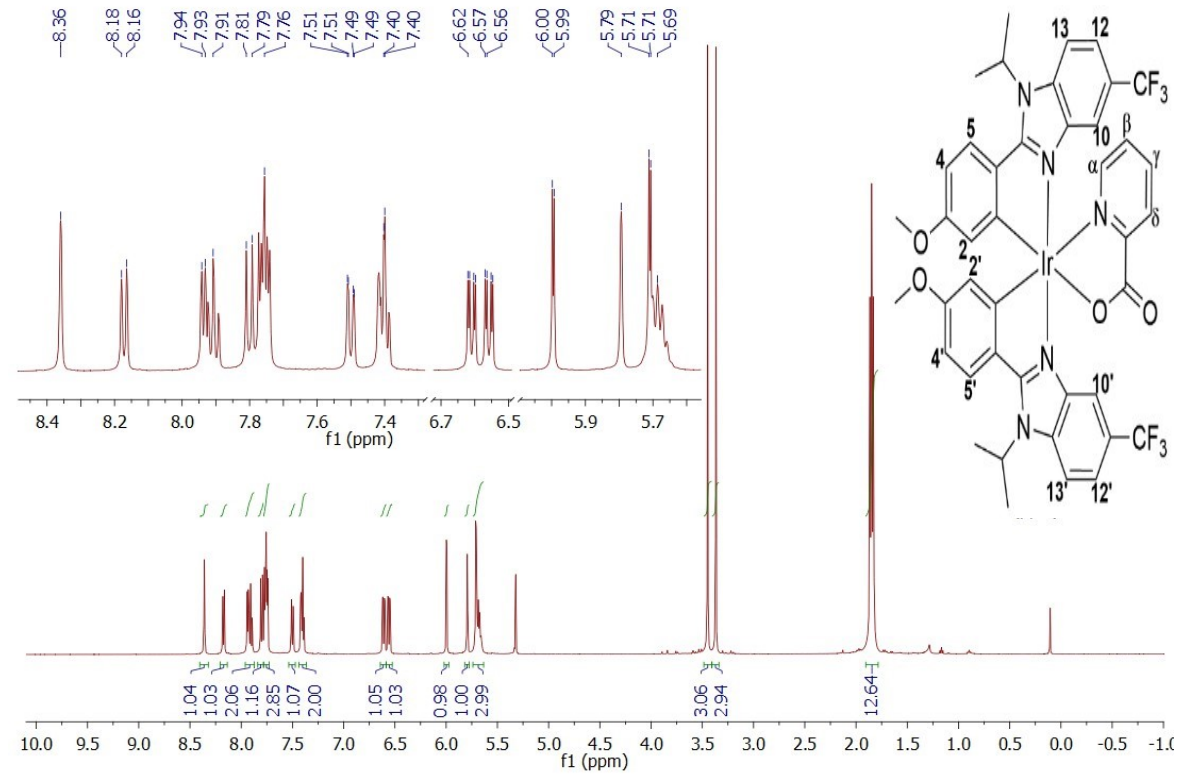

Figure S 24: ^1H NMR spectra (500 MHz, CD_2Cl_2)

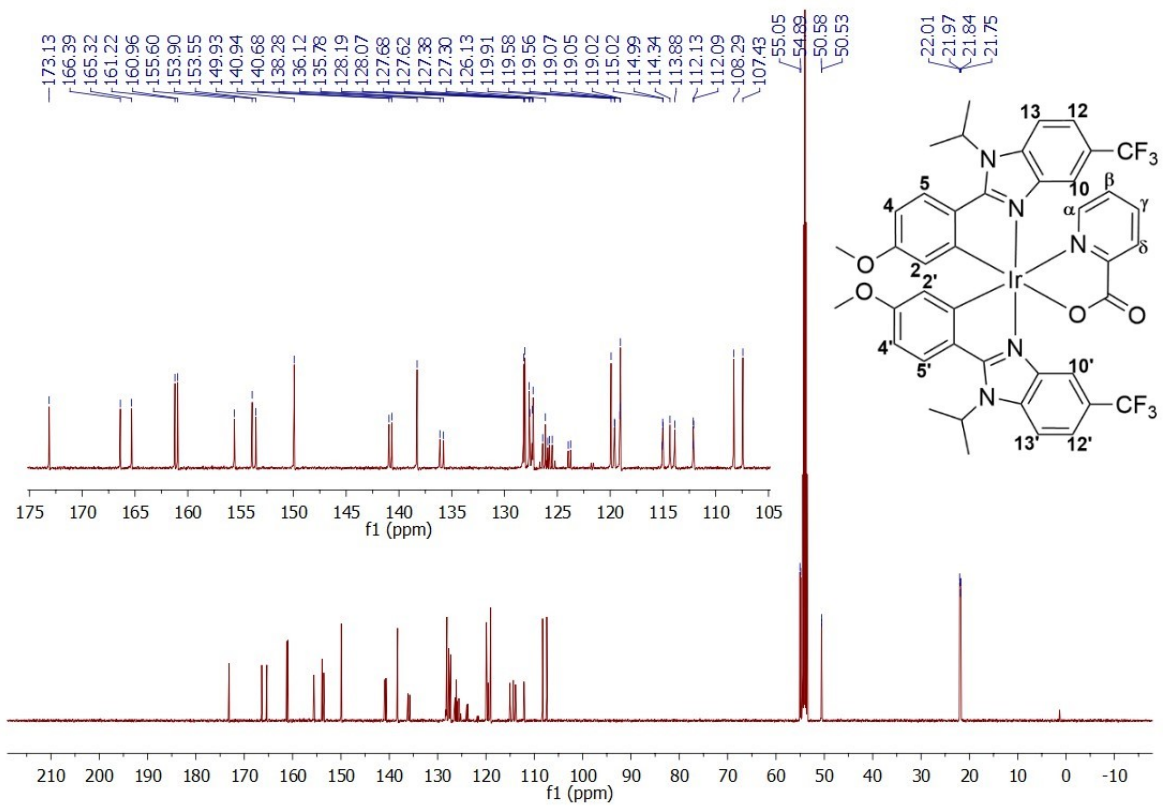

Figure S 25: ^{13}C NMR spectra (500 MHz, CD_2Cl_2)

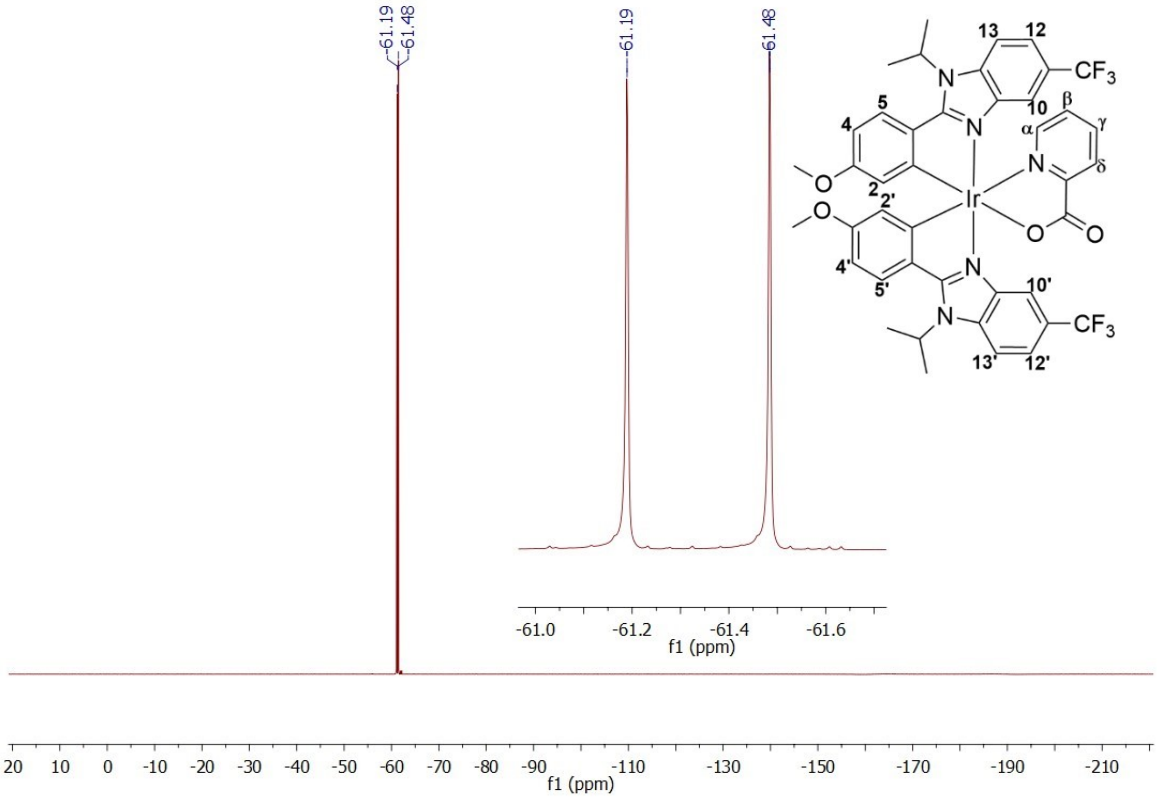

Figure S 26: ^{19}F NMR spectra (500 MHz, CD_2Cl_2)

IrL^{10}_2

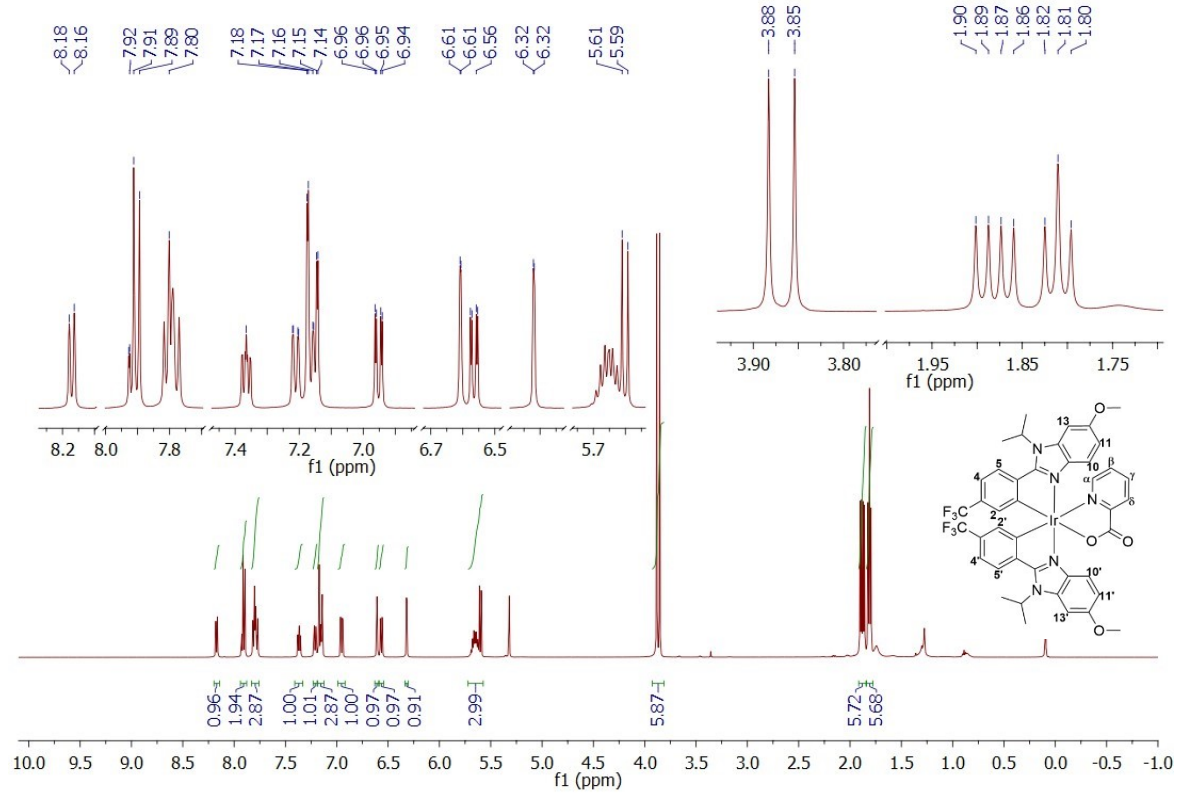

Figure S 27: ^{1}H NMR spectra (500 MHz, CD_2Cl_2)

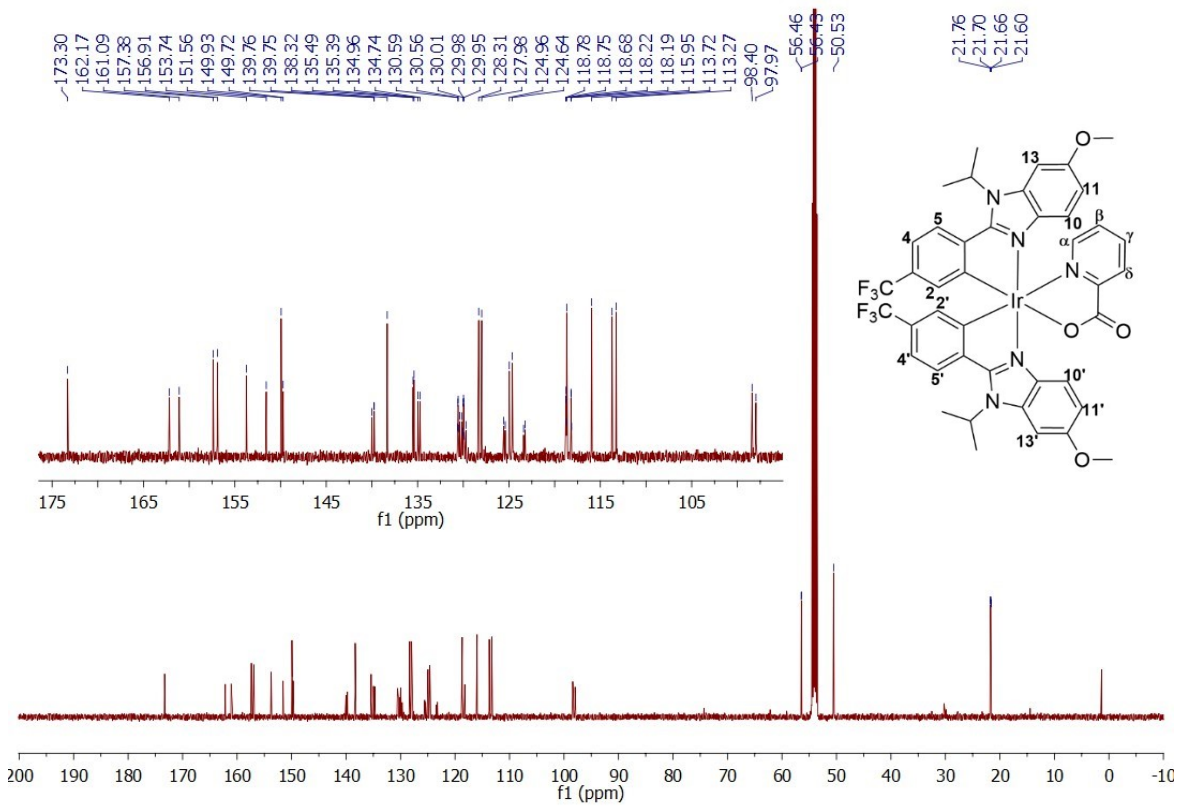

Figure S 28: ^{13}C NMR spectra (500 MHz, CD_2Cl_2)

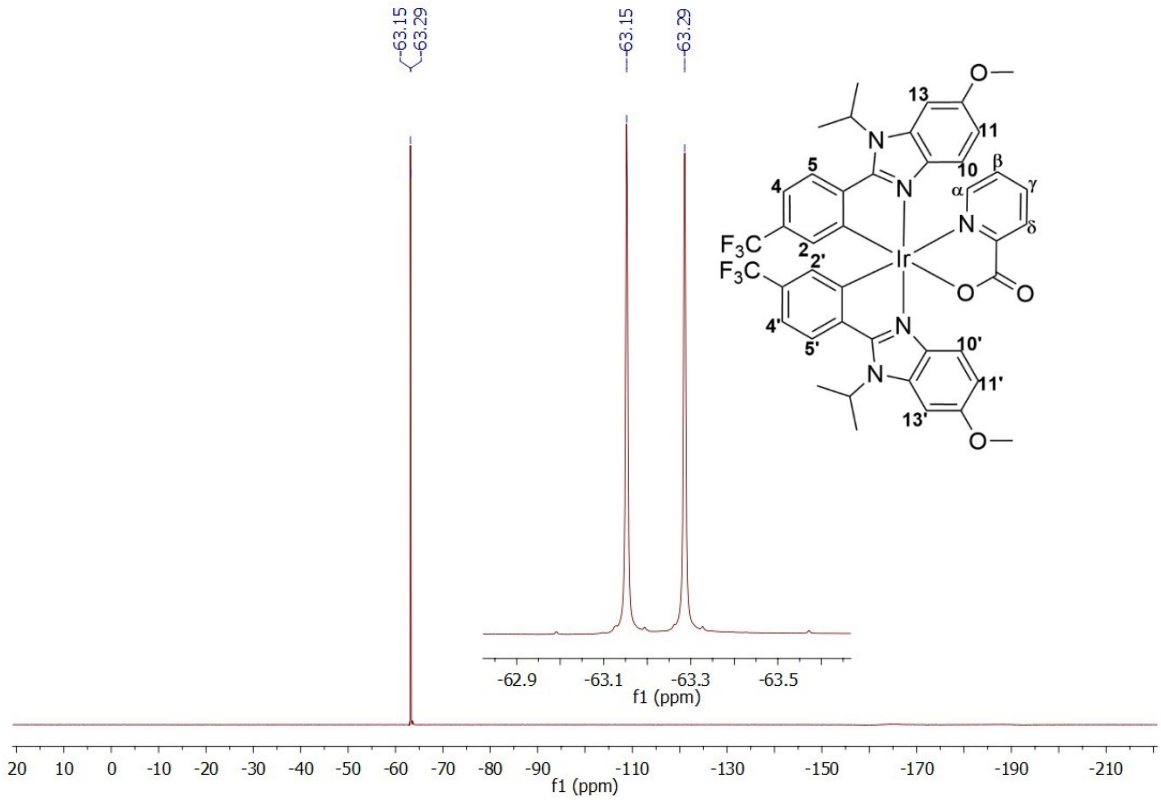

Figure S 29: ^{19}F NMR spectra (500 MHz, CD_2Cl_2)

Figure S 30. Molecular orbital diagrams of the different species

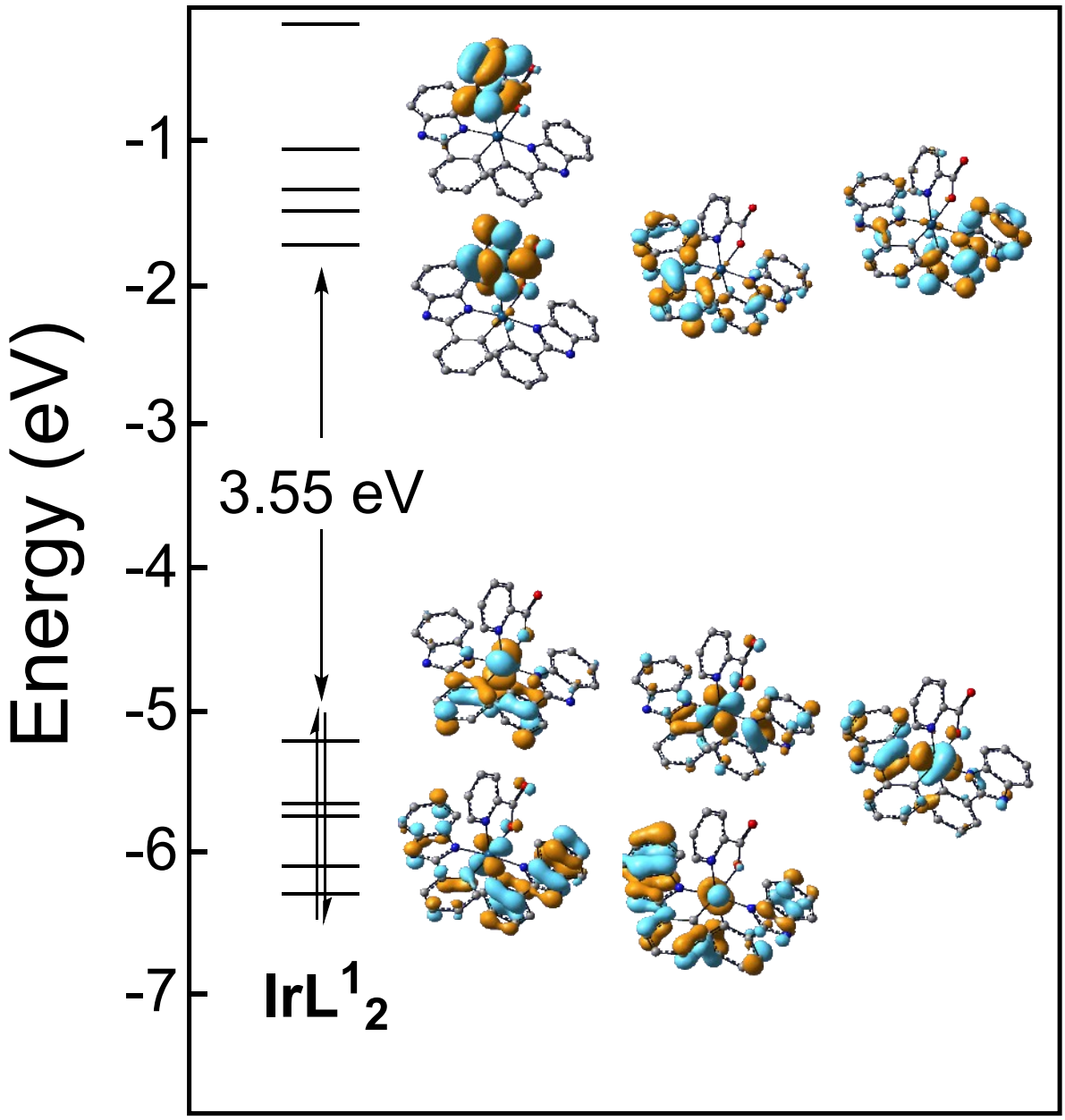

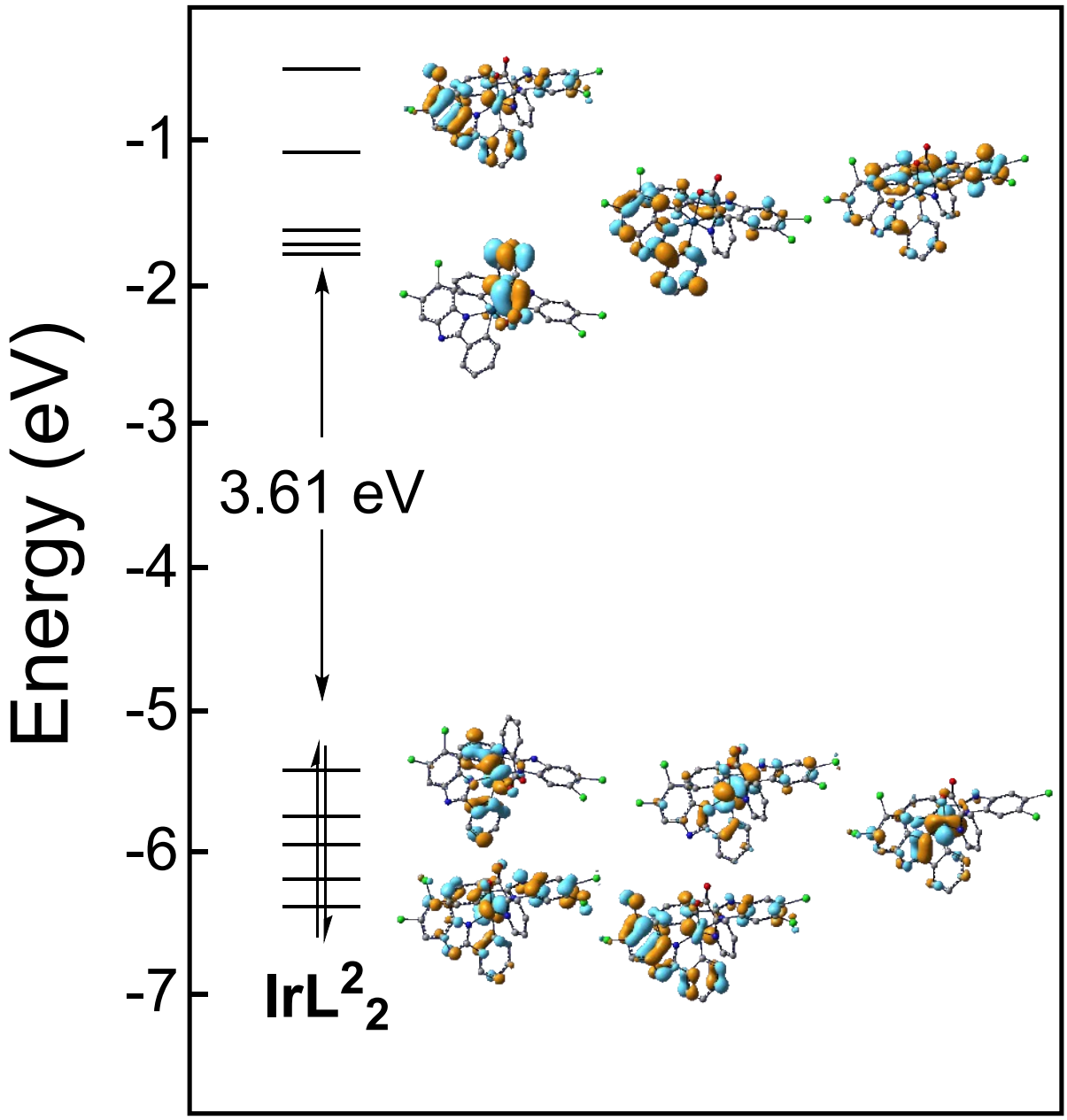
Energy (eV)
-1
-2
-3
-4
-5
-6
-7
3.61 eV
IrL$^2_2$

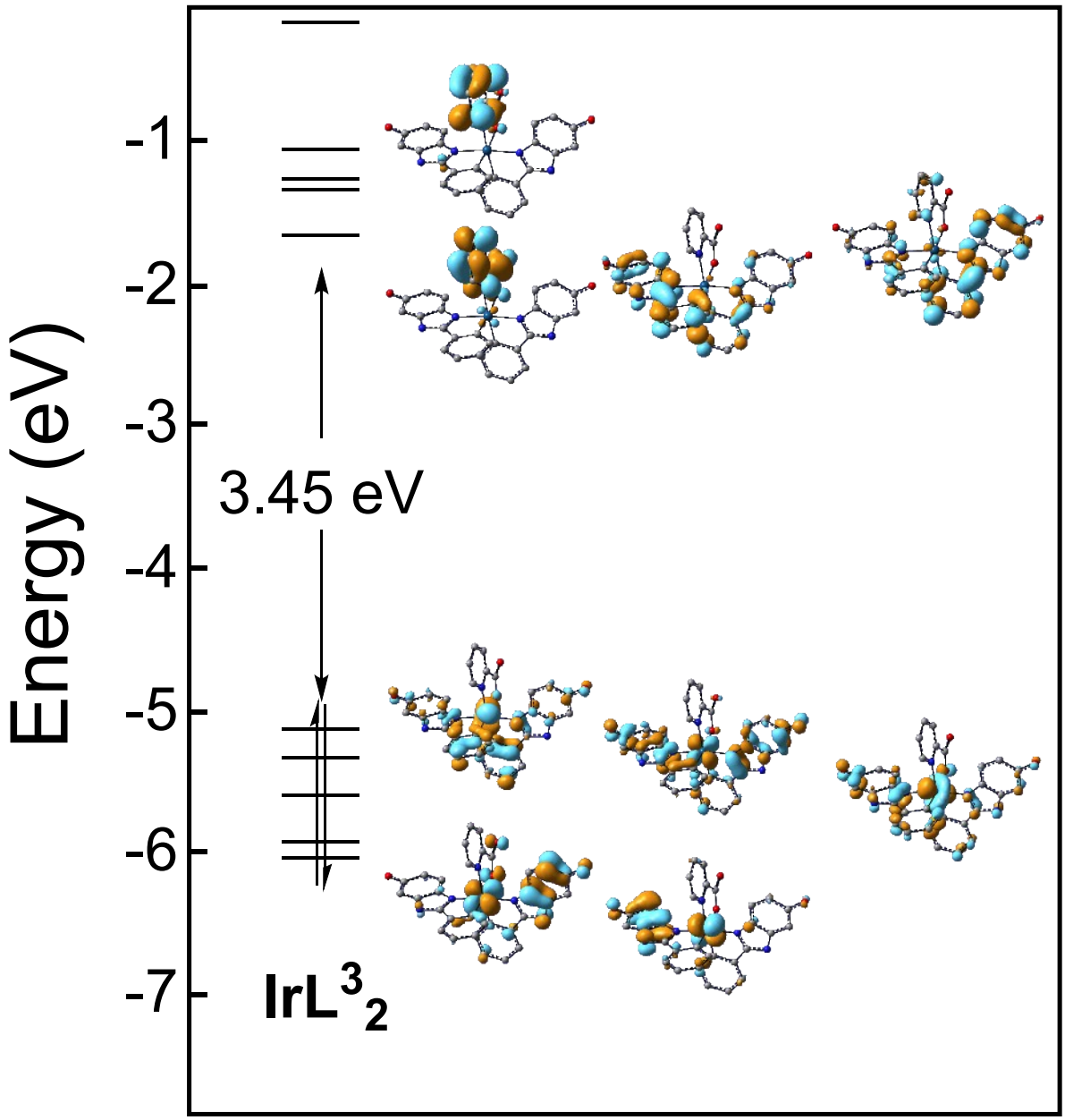
Energy (eV)
-1
-2
-3
-4
-5
-6
-7
3.45 eV
IrL$^3_2$

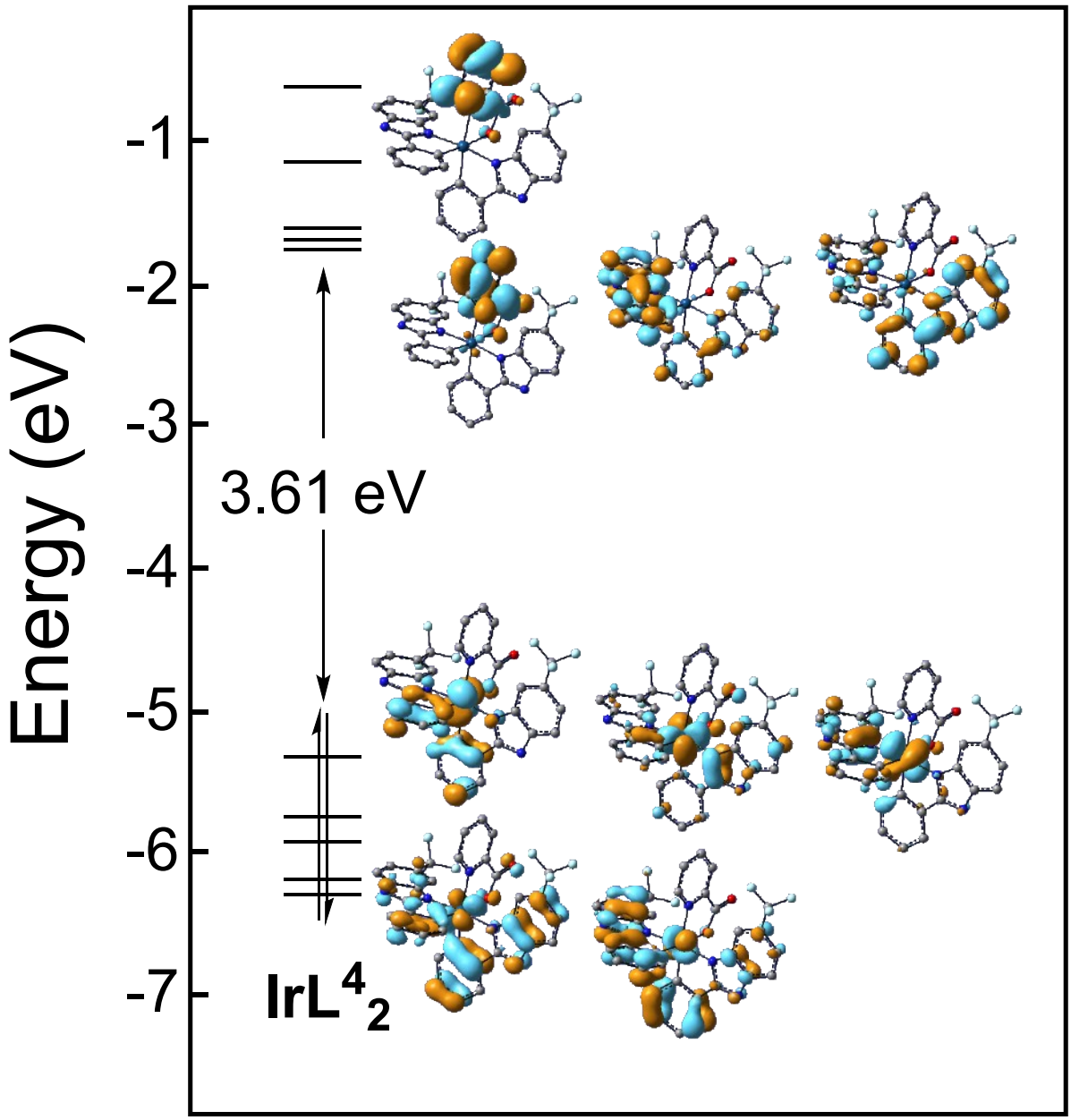
Energy (eV)
-1
-2
-3
-4
-5
-6
-7
3.61 eV
IrL42

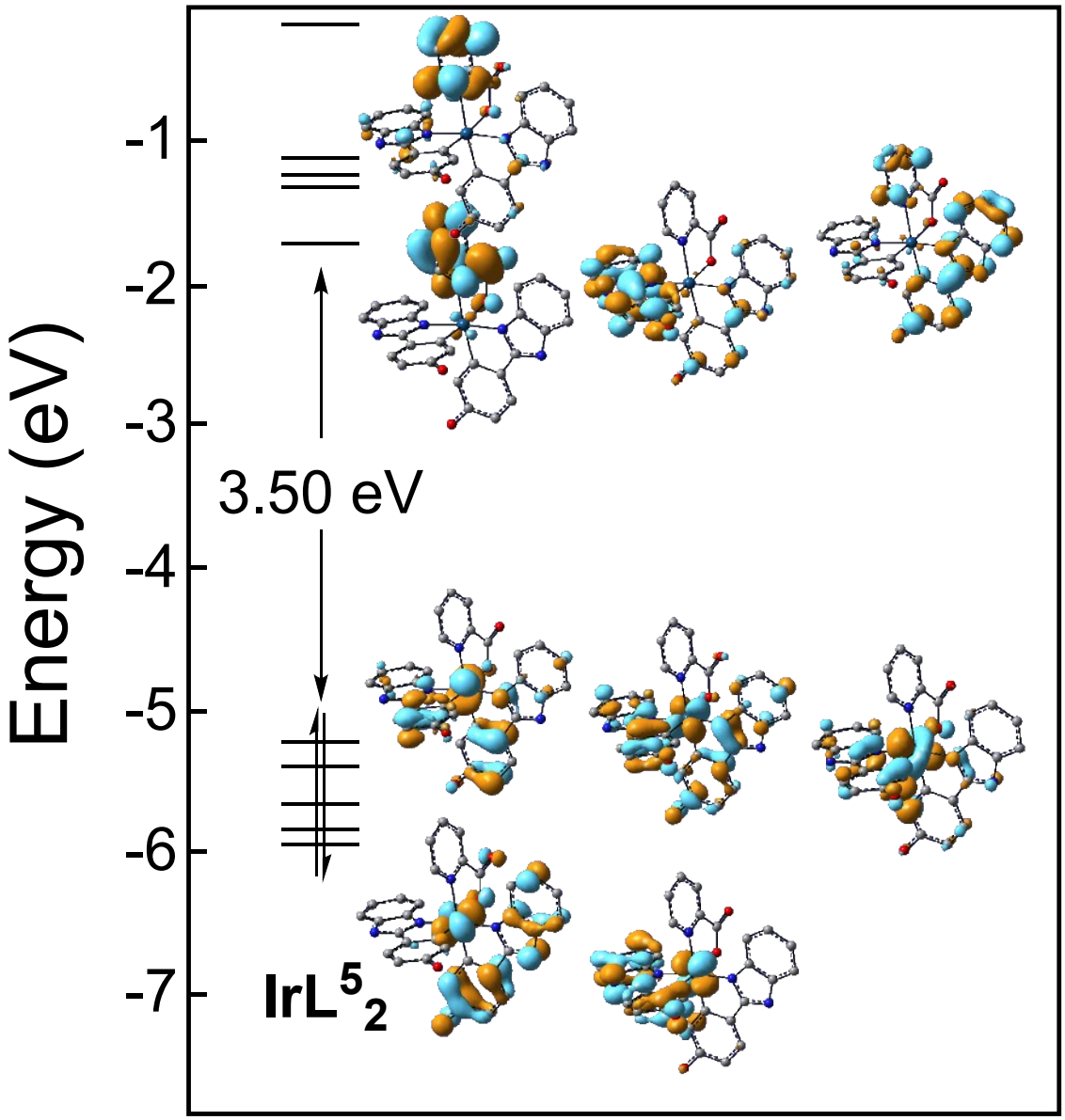
Energy (eV)
-1
-2
-3
-4
-5
-6
-7
3.50 eV
IrL5 2

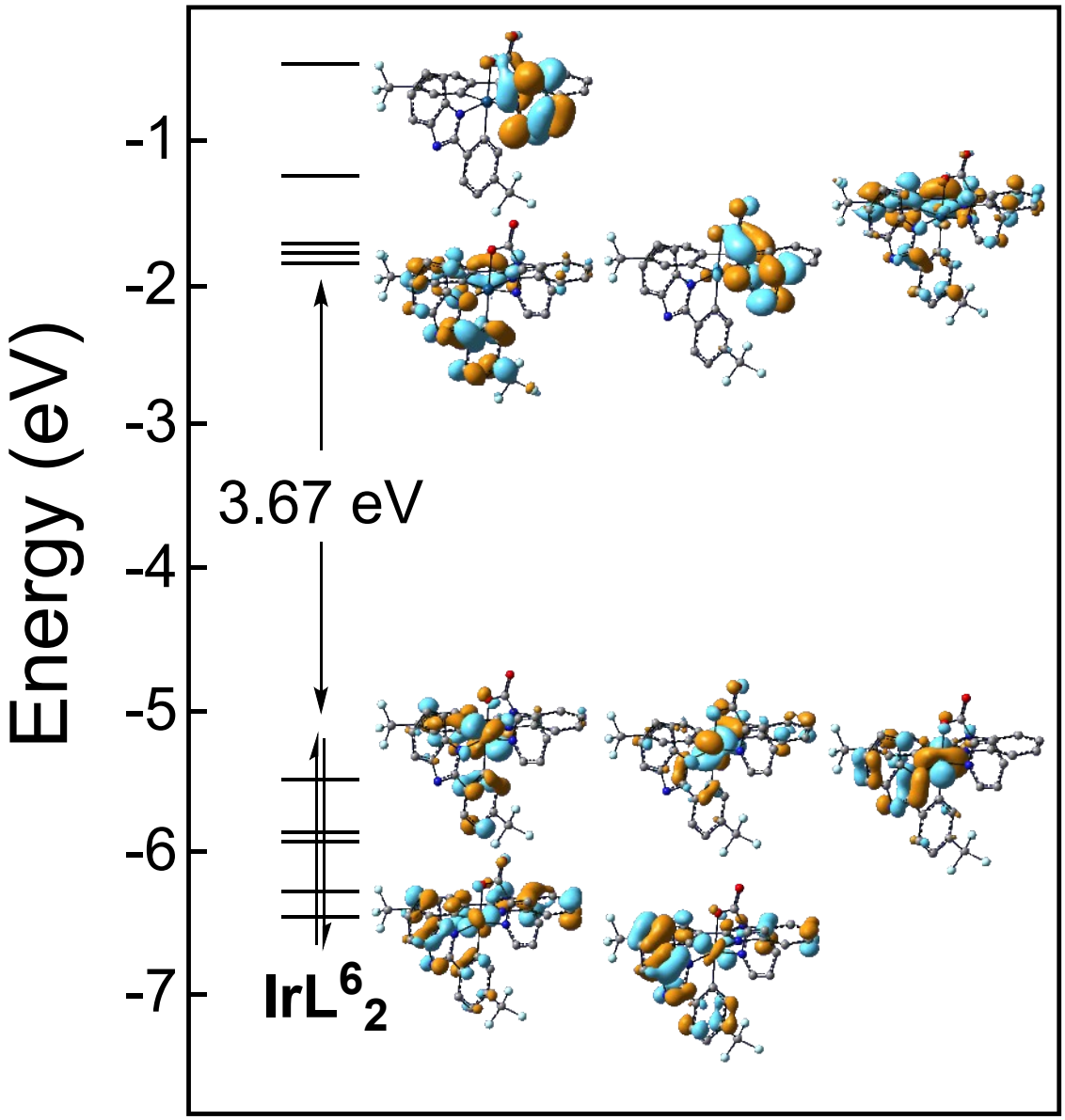
Energy (eV)
-1
-2
-3
-4
-5
-6
-7
3.67 eV
IrL6 2

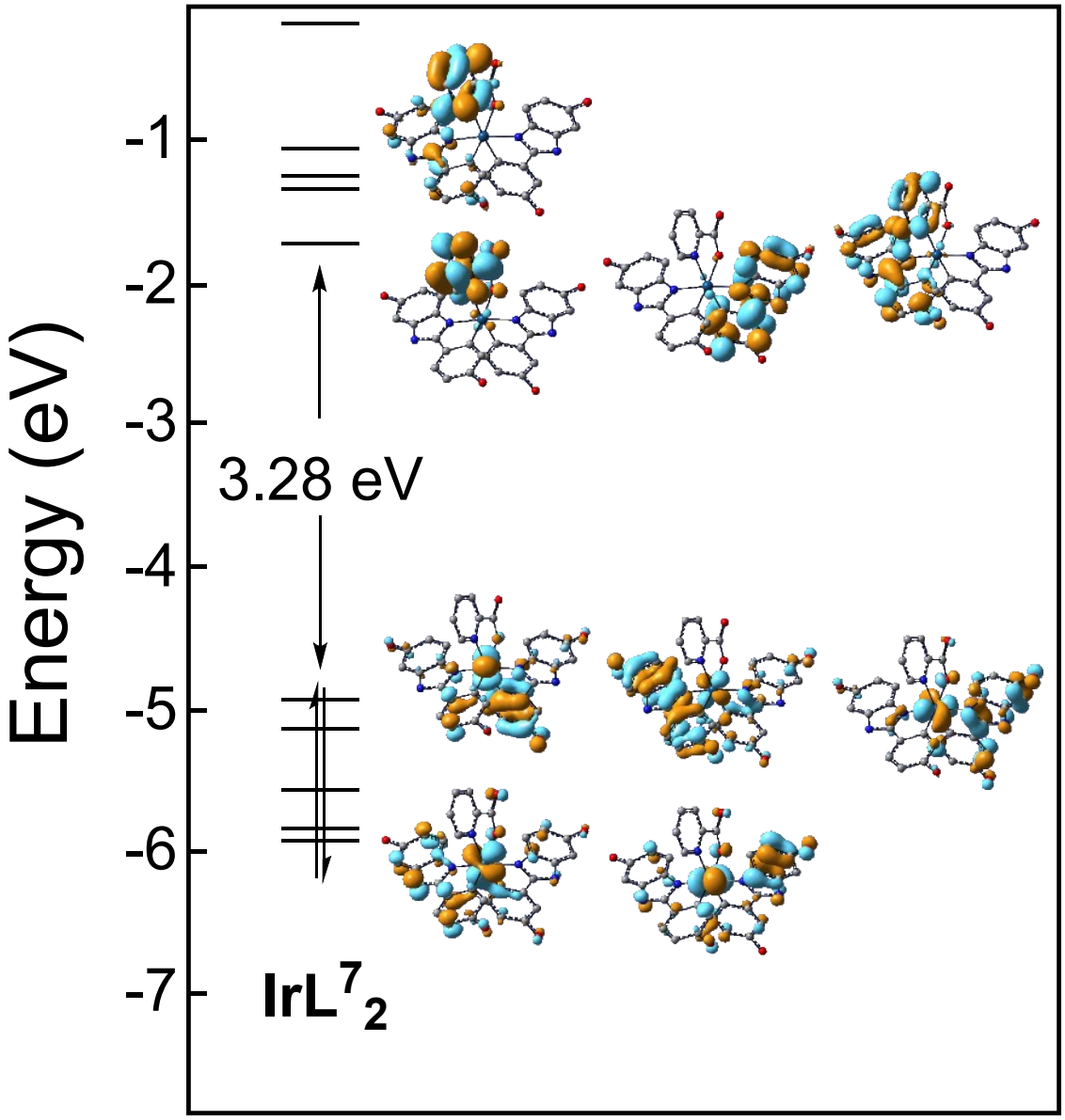
Energy (eV)
-1
-2
-3
-4
-5
-6
-7
3.28 eV
IrL7 2

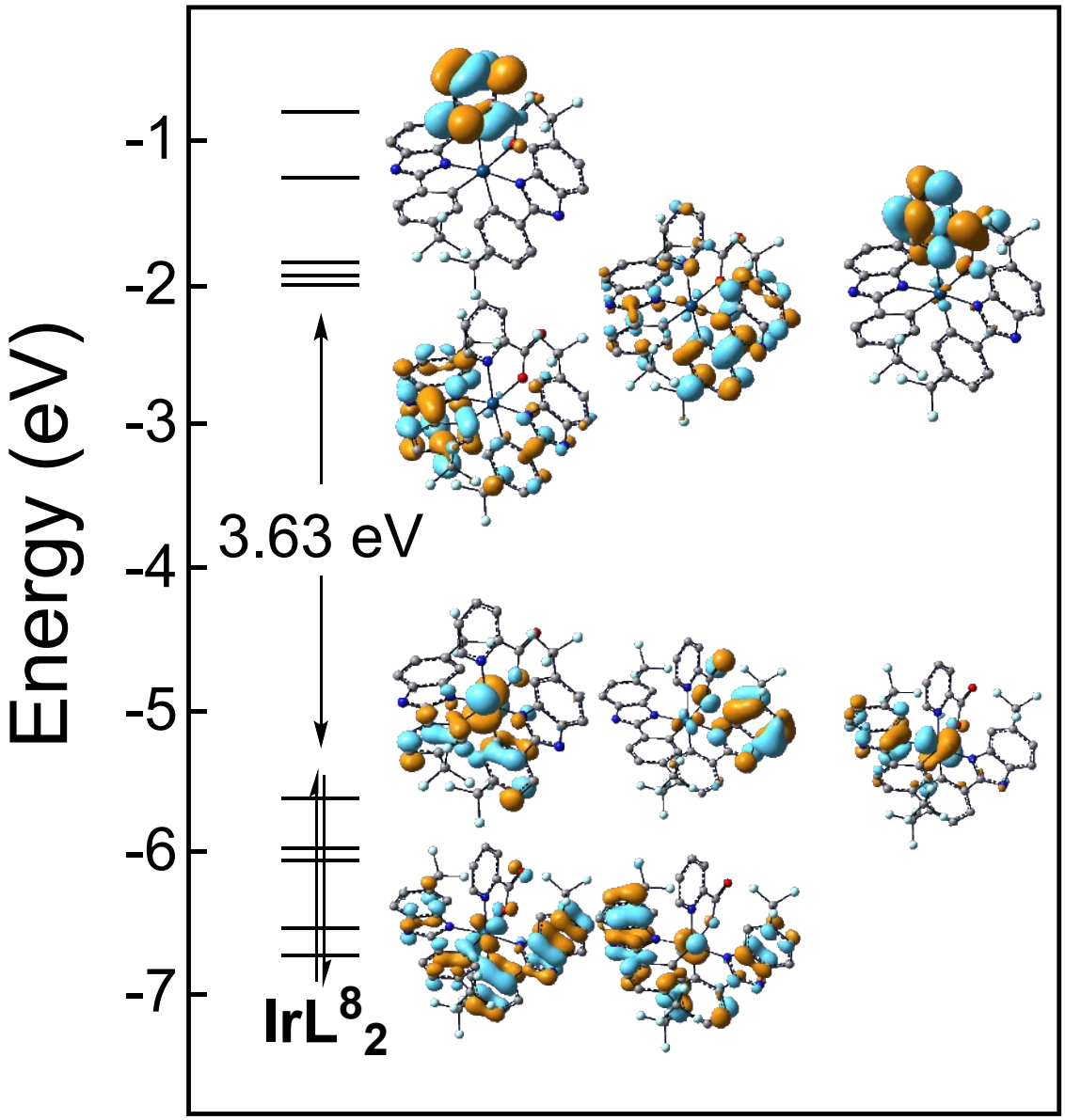
Energy (eV)
-1
-2
-3
-4
-5
-6
-7
3.63 eV
IrL8 2

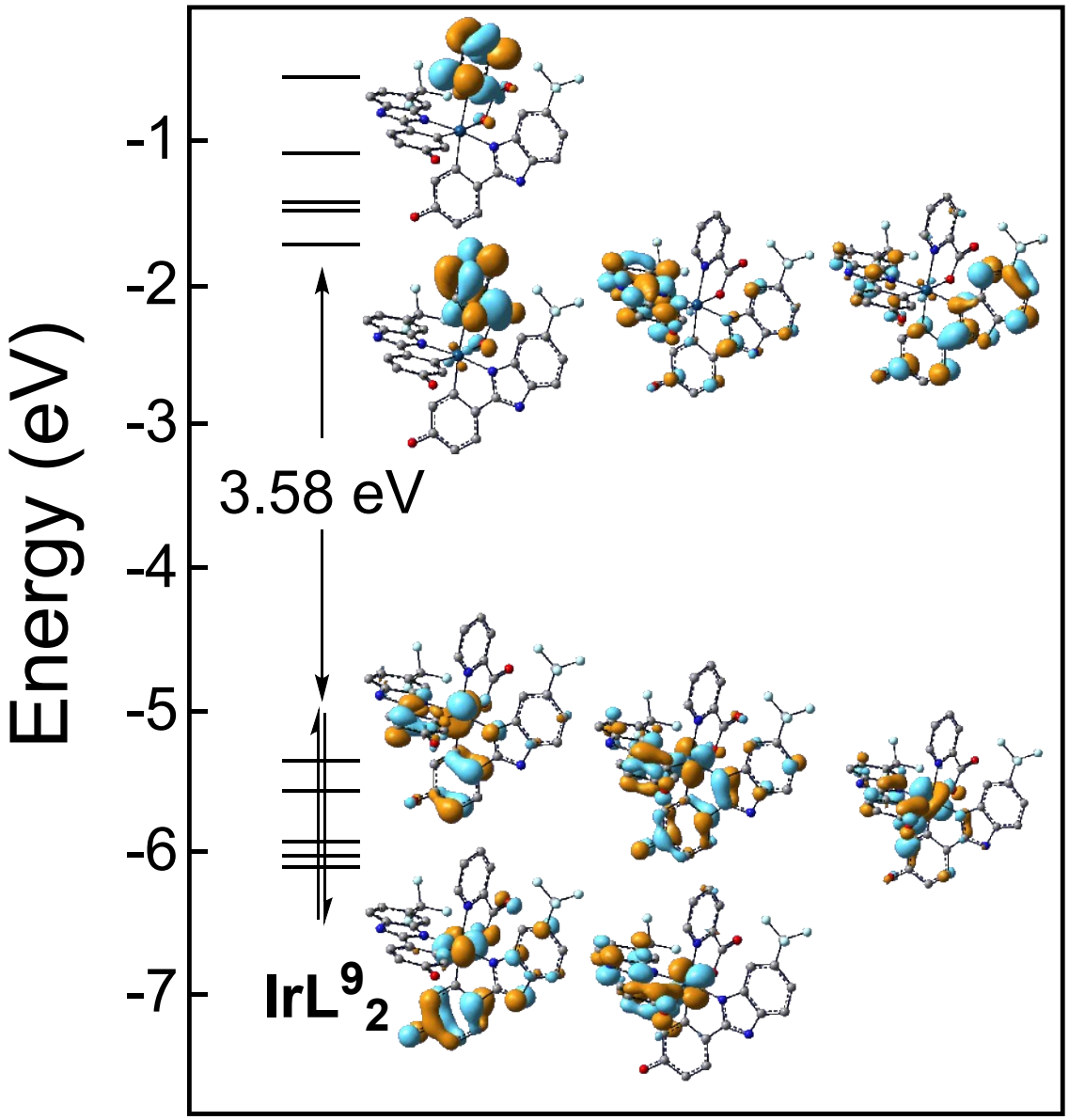
Energy (eV)
-1
-2
-3
-4
-5
-6
-7
3.58 eV
IrL9 2

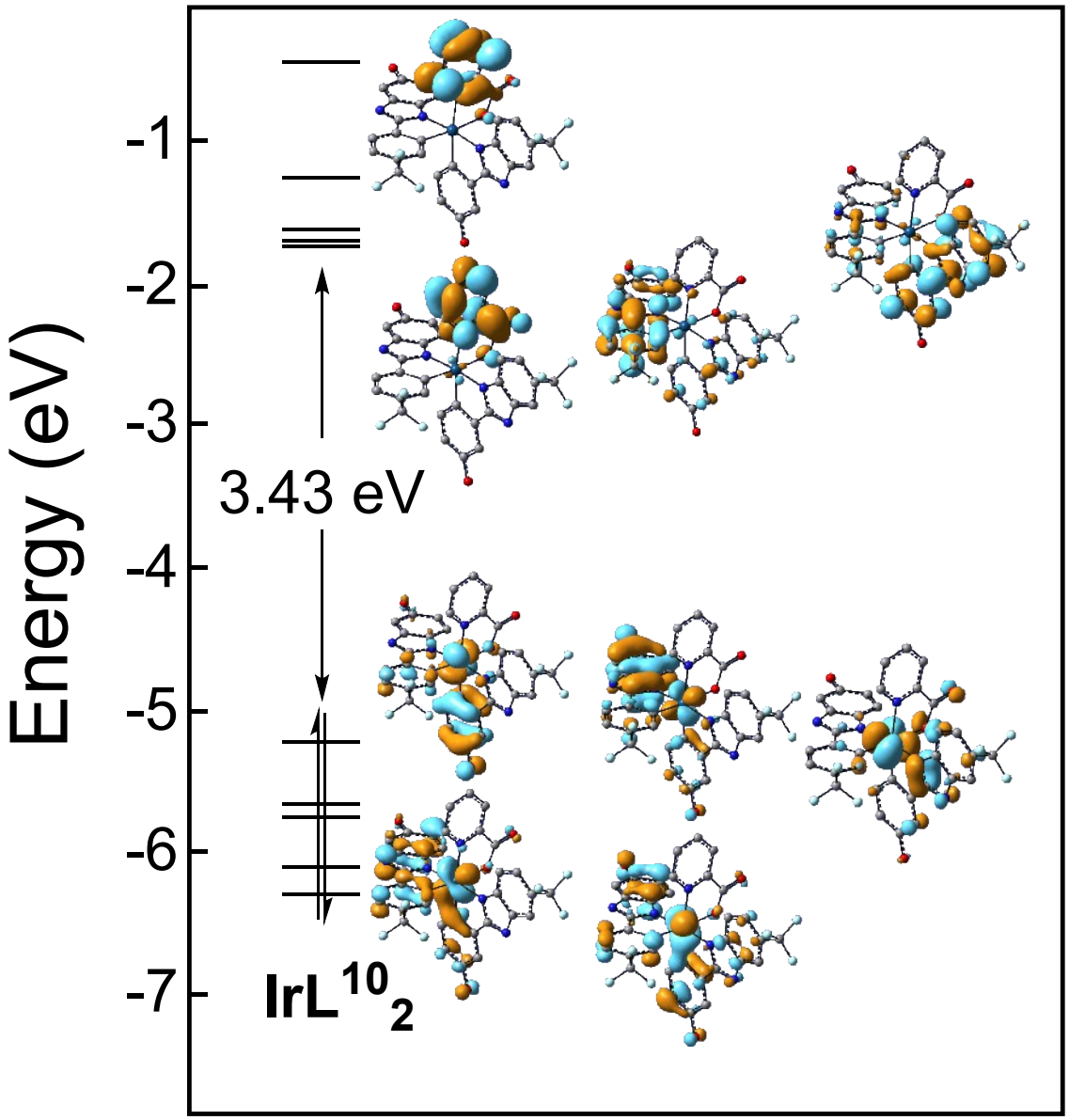
Energy (eV)
-1
-2
-3
-4
-5
-6
-7
3.43 eV
IrL10 2

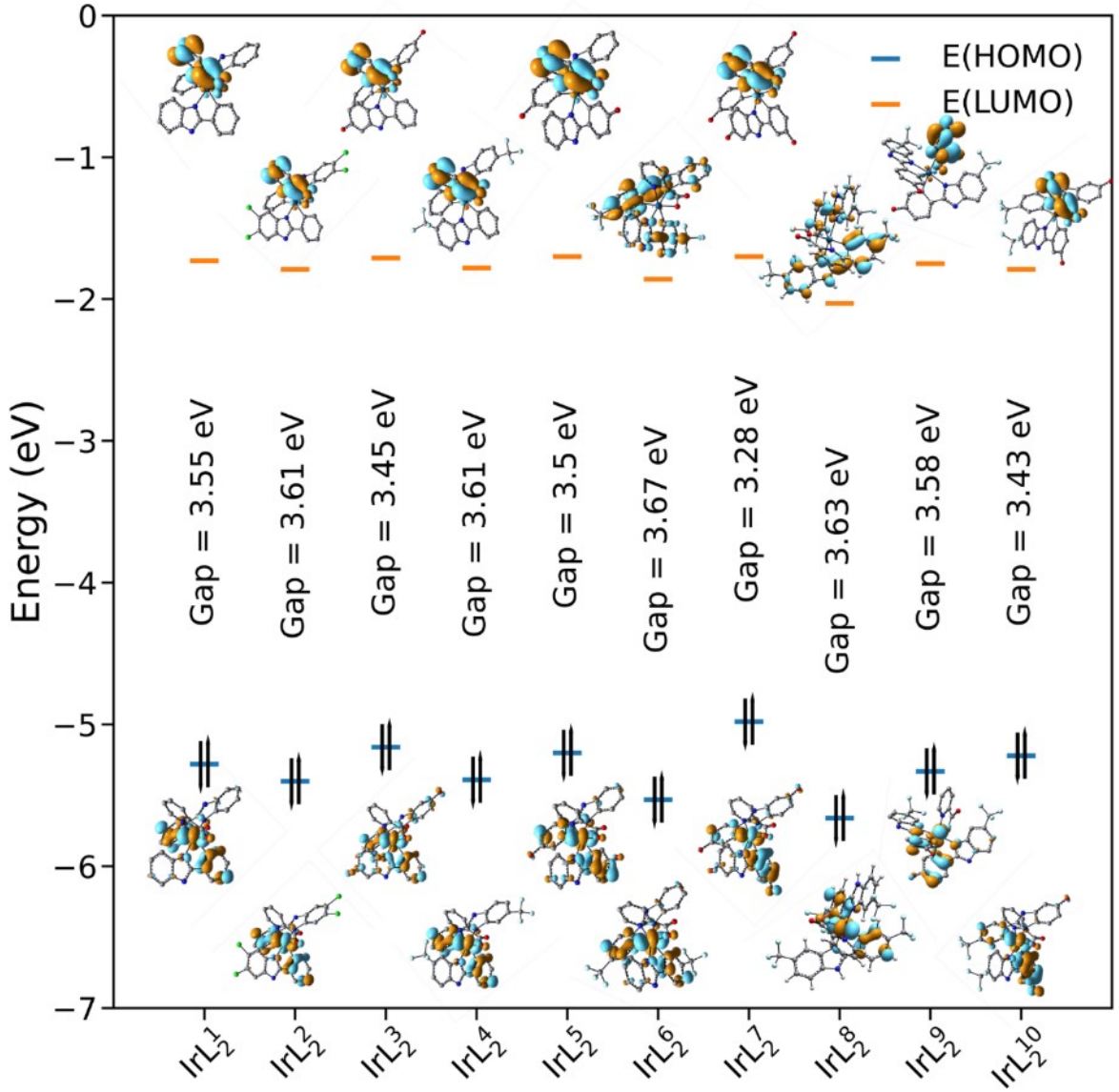

Figure S 31. HOMO-LUMO gap and orbitals for all complexes.

Table S 2. TD-DFT results and absorption band assignments.

Cpd	Transition* (f)	E(eV)	λ(nm)	Assignement
IrL^1_2	HOMO→ LUMO 0.003	2.83	438	ML'CT + LL'CT**
	HOMO→ LUMO+1 0.196	3.04	408	**MLCT + LLCT**
IrL^2_2	HOMO→ LUMO 0.008	2.90	428	ML'CT + LL'CT
	HOMO→ LUMO+1 0.221	2.94	421	**MLCT + LLCT**
IrL^3_2	HOMO→ LUMO 0.004	2.76	450	ML'CT + LL'CT
	HOMO→ LUMO+1 0.223	3.04	408	**MLCT + LLCT**
IrL^4_2	HOMO→ LUMO 0.004	2.90	428	ML'CT + LL'CT
	HOMO→ LUMO+1 0.223	2.97	418	**MLCT + LLCT**
IrL^5_2	HOMO→ LUMO 0.004	2.81	442	ML'CT + LL'CT
	HOMO-1→ LUMO 0.003	3.09	402	ML'CT + LL'CT
	HOMO→ LUMO+1 0.263	3.20	387	**MLCT + LLCT**
IrL^6_2	HOMO→ LUMO 0.171	2.94	421	**MLCT + LLCT**
	HOMO→ LUMO+1 0.008	2.99	415	ML'CT + LL'CT
IrL^7_2	HOMO→ LUMO 0.004	2.61	475	ML'CT + LL'CT
	HOMO→ LUMO+1 HOMO-1→ LUMO 0.095	2.95	421	ML'CT + LL'CT + MLCT + LLCT
	HOMO→ LUMO+1 HOMO-1→ LUMO 0.152	2.96	419	**ML'CT + LL'CT + MLCT + LLCT**
IrL^8_2	HOMO→ LUMO 0.159	2.90	427	**MLCT + LLCT**
	HOMO→ LUMO+1 0.015	3.02	411	ML'CT + LL'CT + MLCT + LLCT

IrL^9_2	HOMO→ LUMO 0.004 HOMO→ LUMO+1 0.245	2.89 3.14	430 400	ML'CT + LL'CT **MLCT + LLCT**
IrL^{10}_2	HOMO→ LUMO HOMO→ LUMO+1 0.018 HOMO→ LUMO HOMO→ LUMO+1 0.165 HOMO→ LUMO+2 0.152	2.75 2.78 2.93	450 447 423	ML'CT + LL'CT + MLCT + LLCT ML'CT + LL'CT + MLCT + LLCT **MLCT + LLCT**

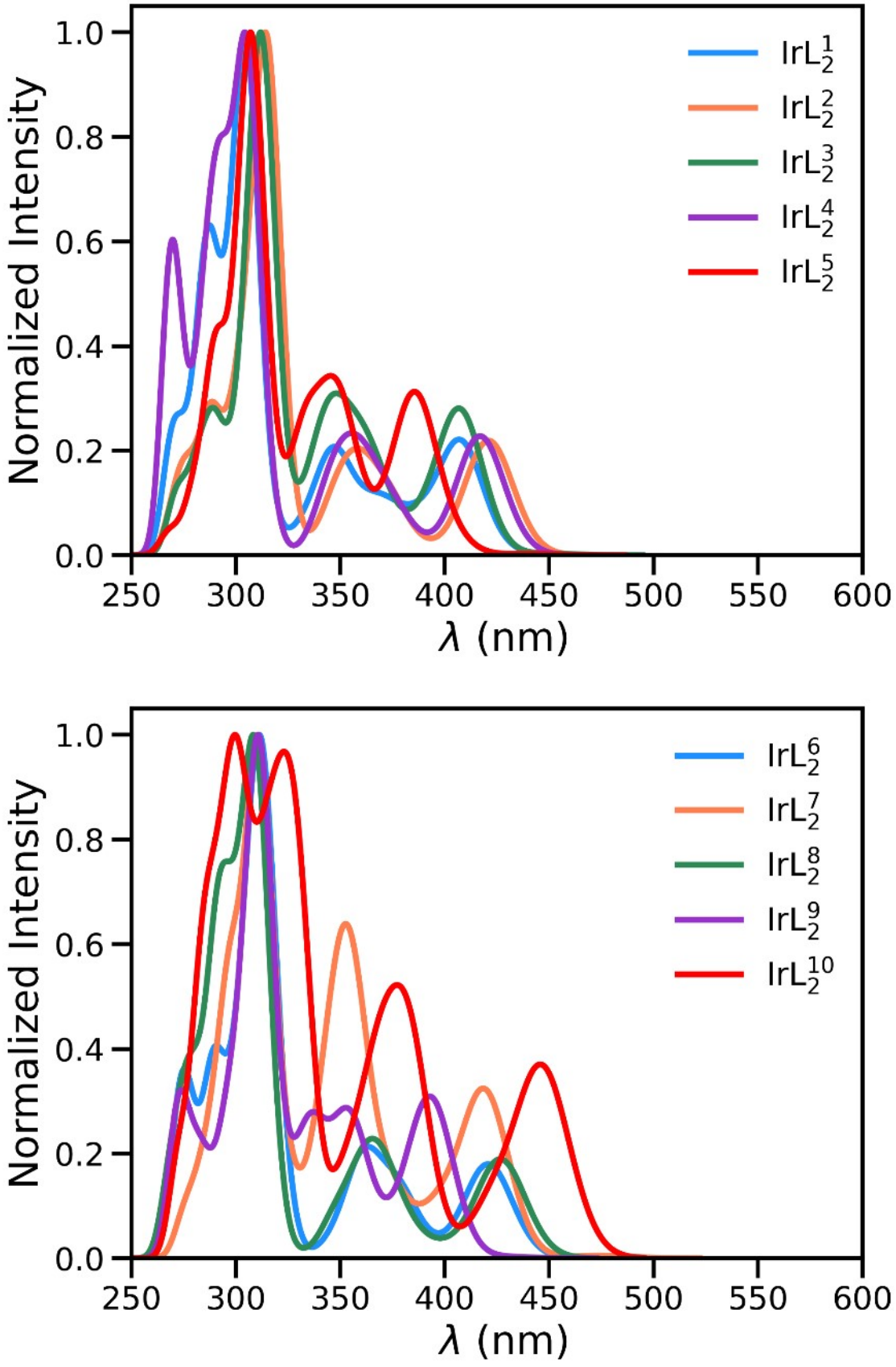

Figure S 32. Simulated absorption spectra using TD-DFT.

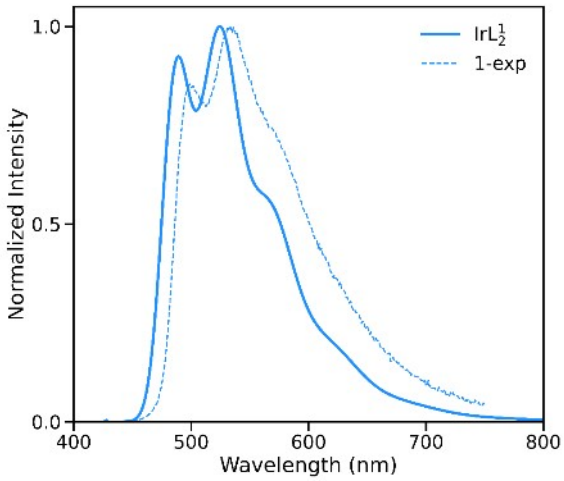
Normalized Intensity
Wavelength (nm)
IrL$_2^1$
1-exp

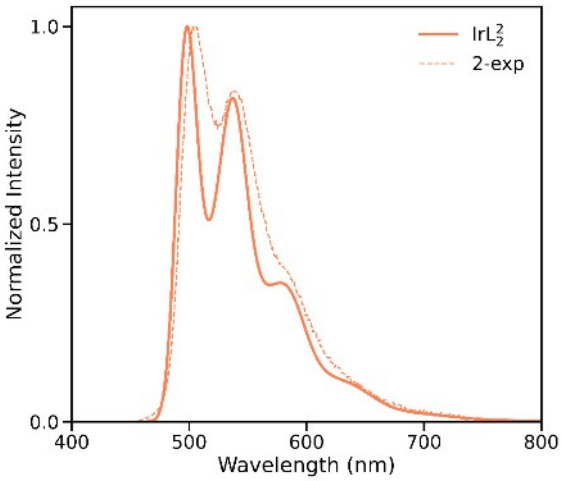
Normalized Intensity
Wavelength (nm)
IrL$_2^2$
2-exp

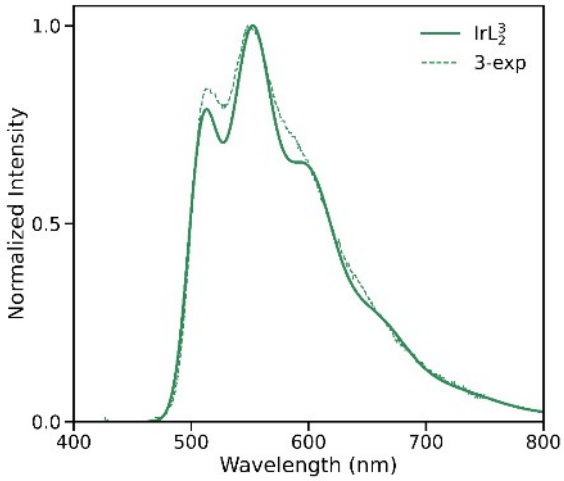
Normalized Intensity
Wavelength (nm)
IrL$_2^3$
3-exp

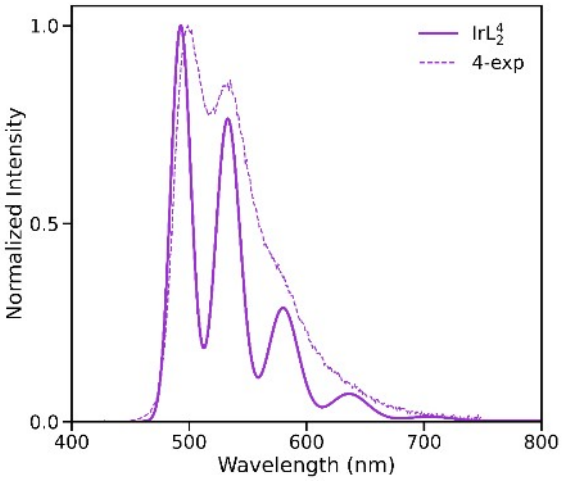
Normalized Intensity
Wavelength (nm)
IrL$_2^4$
4-exp

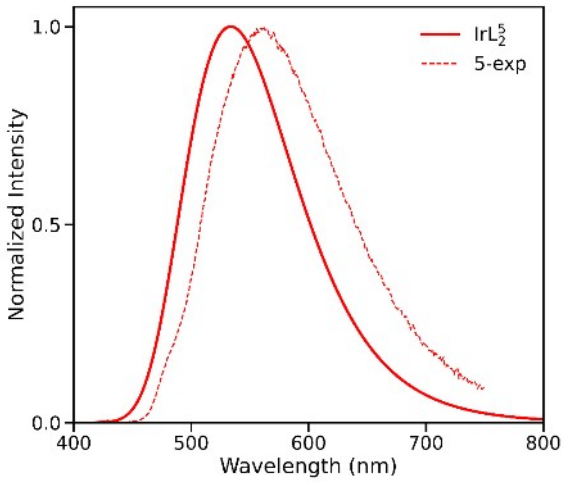
Normalized Intensity
Wavelength (nm)
IrL$_2^5$
5-exp

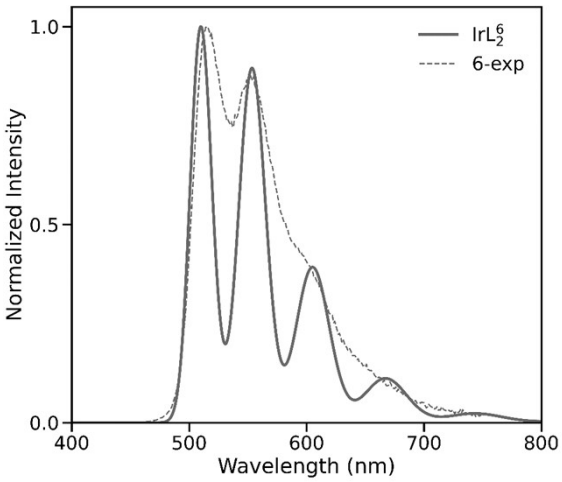
Normalized Intensity
Wavelength (nm)
IrL$_2^6$
6-exp

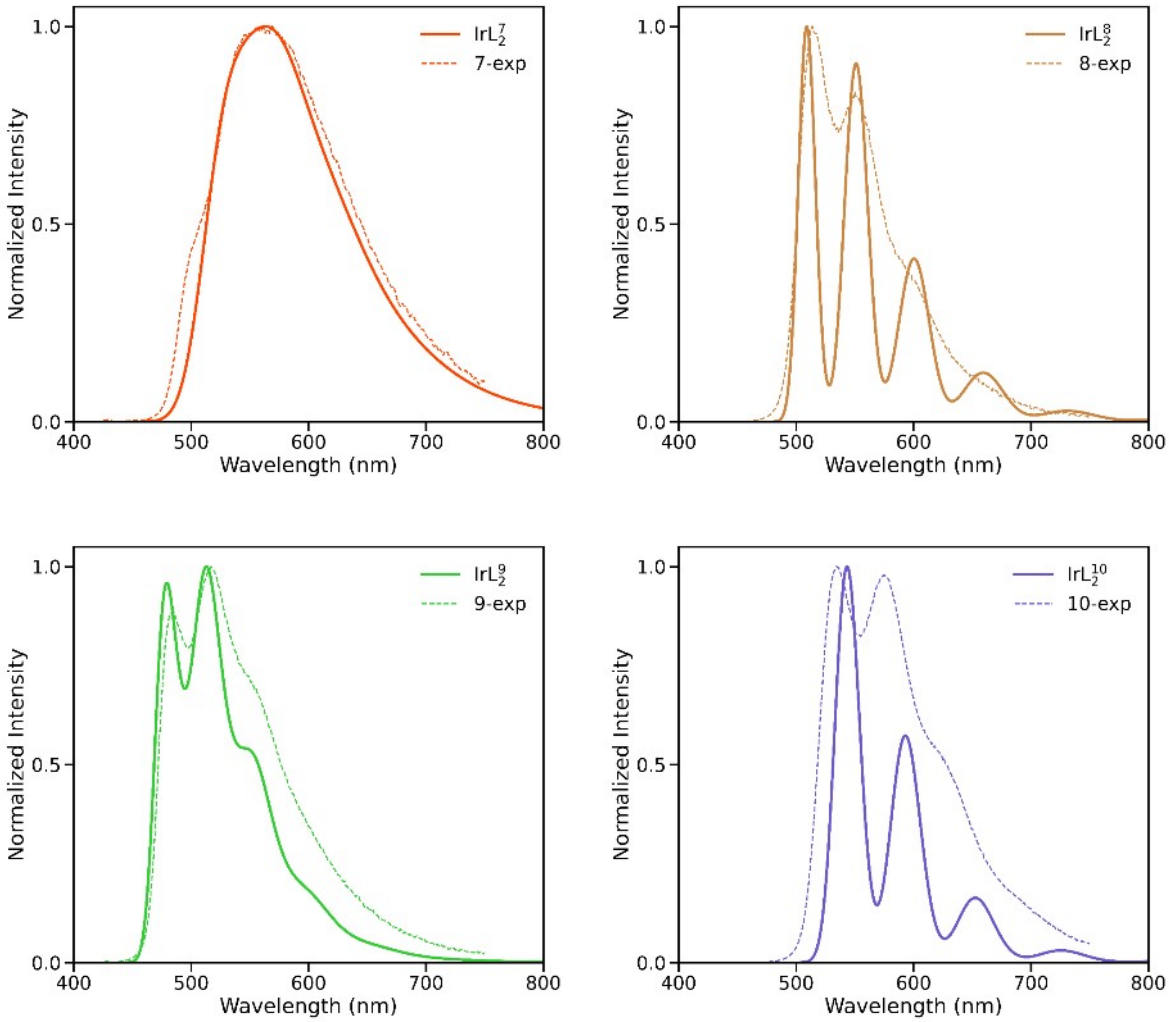

Figure S 33. Recorded (RT) and simulated phosphorescence spectra.

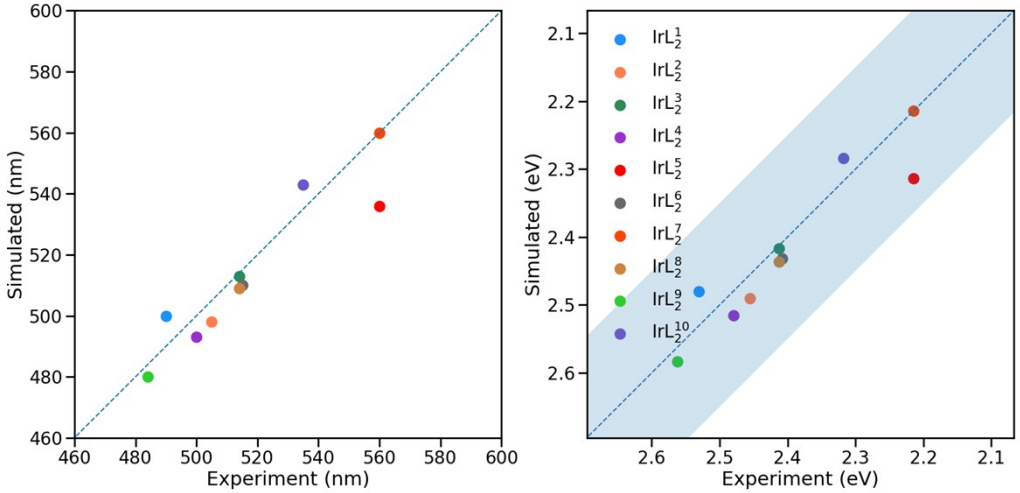

Figure S 34. Correlation between the simulated and recorded luminescence at RT.

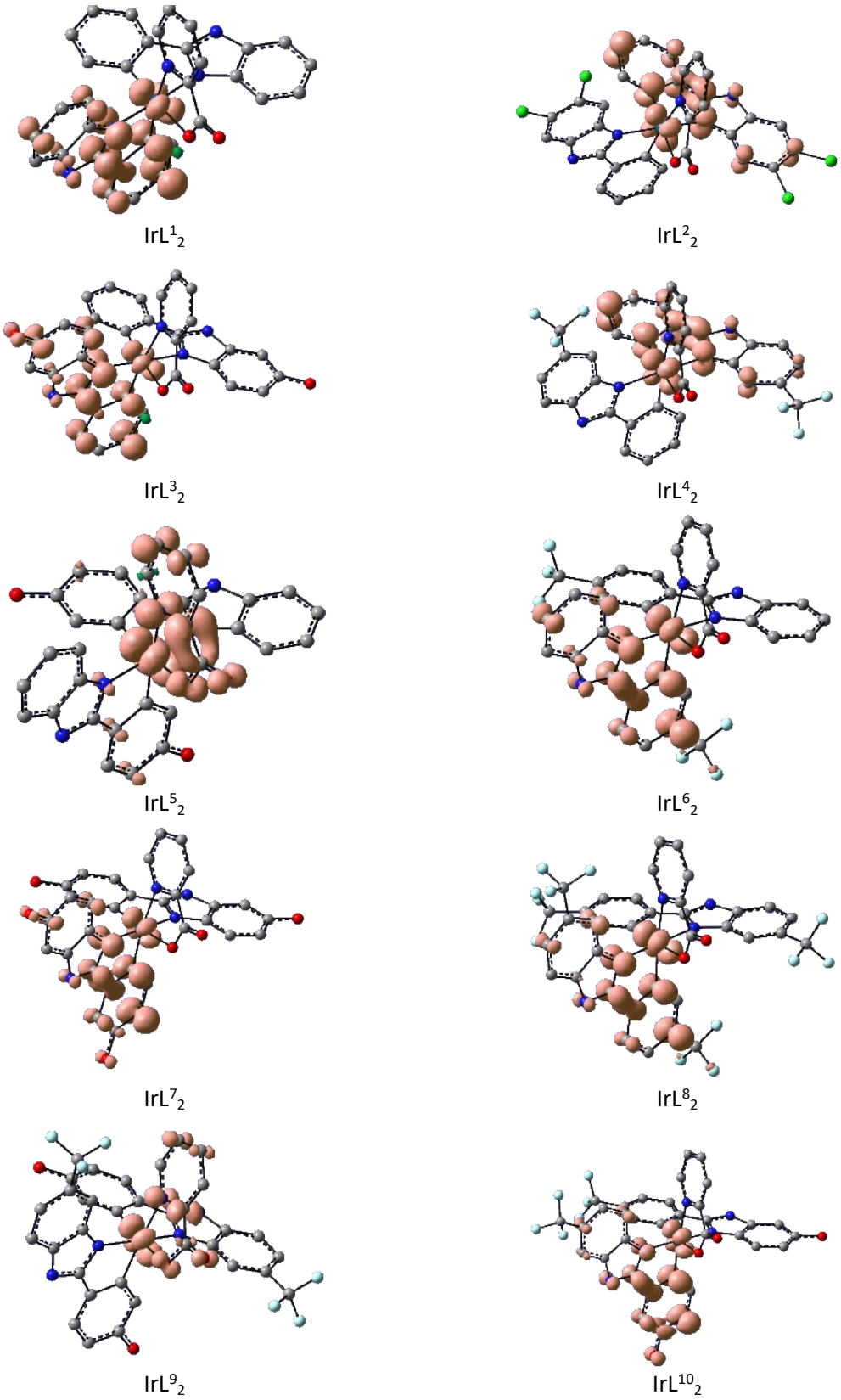

Figure S 35. Spin density localization of each complex in the excited state.

References

1. Duisenberg, A. J. M., Kroon-Batenburg, L. M. J. & Schreurs, A. M. M. An intensity evaluation method: EVAL-14. *J. Appl. Crystallogr.* **36**, 220–229 (2003).

2. Sheldrick, G. M. Crystal structure refinement with SHELXL. *Acta Crystallogr. Sect. C Struct. Chem.* **71**, 3–8 (2015).

3. Dolomanov, O. V., Bourhis, L. J., Gildea, R. J., Howard, J. A. K. & Puschmann, H. OLEX2: A complete structure solution, refinement and analysis program. *J. Appl. Crystallogr.* **42**, 339–341 (2009).

4. Tamura, Y., Hisamatsu, Y., Kumar, S., Itoh, T., Sato, K., Kuroda, R. & Aoki, S. Efficient Synthesis of Tris-Heteroleptic Iridium(III) Complexes Based on the Zn 2+-Promoted Degradation of Tris-Cyclometalated Iridium(III) Complexes and Their Photophysical Properties. *Inorg. Chem.* **56**, 812–833 (2017).

5. Denisov, S. A., Cudré, Y., Verwilst, P., Jonusauskas, G., Marín-Suárez, M., Fernández-Sánchez, J. F., Baranoff, E. & McClenaghan, N. D. Direct Observation of Reversible Electronic Energy Transfer Involving an Iridium Center. *Inorg. Chem.* **53**, 2677–2682 (2014).

6. Yao, S., Ou, Y. & Ye, B. Asymmetric Synthesis of Enantiomerically Pure Mono- and Binuclear Bis(cyclometalated) Iridium(III) Complexes. *Inorg. Chem.* **55**, 6018–6026 (2016).